Transport in Porous Media (2025) 152:12
https://doi.org/10.1007/s11242-024-02148-y

Exploring Effective Diffusion Coefficients in Water-Saturated Reservoir Rocks via the Pressure Decay Technique: Implications for Underground Hydrogen Storage

Saeed Khajooie[1,2] · Garri Gaus[1,4] · Timo Seemann[3] · Benedikt Ahrens[5] · Tian Hua[6] · Ralf Littke[1]

Received: 25 June 2024 / Accepted: 4 December 2024 / Published online: 8 January 2025

Abstract

The assessment of gas diffusion in water-saturated rocks is essential for quantifying gas loss and determining the amount of gas that could trigger abiotic and biotic processes, potentially altering fluid and rock properties. Additionally, estimating diffusion coefficients is critical for evaluating the balance between hydrogen generation and dissipation in radioactive waste repositories. This investigation involved experimental determination of diffusion coefficients for various gases both in water and in water-saturated Bentheim, Oberkirchner, Grey Weser, and Red Weser sandstones. Experimental conditions included pressures ranging from 0.2 to 1.0 MPa, consistently maintained at a temperature of 35 °C. The diffusion coefficients of hydrogen, helium, and methane in water were determined to be $6.7{\cdot}10^{-9}$, $9.6{\cdot}10^{-9}$, and $2.8{\cdot}10^{-9}$ m^2/s, respectively, consistent with literature values obtained through gas concentration measurements without pressure gradients. However, the diffusivity of carbon dioxide and argon in water was measured at $10.9{\cdot}10^{-9}$ and $44.6{\cdot}10^{-9}$ m^2/s, significantly exceeding their corresponding literature values by an order of magnitude. This discrepancy is attributed to the significant solubility of these gases in water, resulting in density-driven convection as the primary transport mechanism. Furthermore, the effective diffusion coefficients for hydrogen within the analyzed rock specimens varied from $0.8{\cdot}10^{-9}$ to $2.9{\cdot}10^{-9}$ m^2/s, which are higher than those for methane and carbon dioxide, both ranging from $0.3{\cdot}10^{-9}$ to $0.9{\cdot}10^{-9}$ m^2/s. This yielded diffusive tortuosity values ranging from 2.6 to 8.2. The observed effective diffusivity values were positively correlated with porosity, permeability, and mean pore size, while exhibiting a negative correlation with tortuosity. Given that the gas–liquid mass transfer coefficient is directly proportional to the effective gas diffusivity in water, the determined values for H_2 are essential for studying the impact of pore characteristics on microbial activity.

Highlights

- H_2, CH_4, and CO_2 effective diffusivities were measured on reservoir analogues.
- Effective diffusivities correlate with porosity, permeability, and mean pore size.
- Pressure decay reliability was proven by replicating H_2 and CH_4 diffusivity in water.

Extended author information available on the last page of the article

Keywords Diffusion coefficient · Pressure decay · Tortuosity · Effective diffusivity · Underground hydrogen storage

1 Introduction

Molecular diffusion plays a crucial role in assessing the potential risks or benefits associated with solute transfer through caprocks, reservoir rocks, and wellbore cements during underground storage of natural gas, CO_2, and H_2 in water-saturated porous formations (Charlet et al. 2017; Hanson et al. 2022; Hubao et al. 2024). Moreover, evaluating the diffusion process is essential for ensuring the safe disposal of radioactive waste in geological host rocks (clay formations) or engineered barriers (Jacops et al. 2020).

During the gas storage phase, once the injected gas reaches pressure equilibrium within the reservoir, diffusion is the primary mode of gas transport within reservoirs, highlighting its critical role in ensuring effective gas storage (Jacops et al. 2020; Song and Zhang 2013). Gas molecules are recognized to diffuse through the water-filled pore space of cap rocks, but the rates of this process remain controversial (Krooss et al. 1988; Wollenweber et al. 2009). Investigating the diffusive loss through caprock is essential for assessing its integrity during prolonged subsurface gas storage (Michelsen et al. 2022). In addition, gas dissolution and diffusion in the underlying aquifers may pose challenges for the storage of natural gas and H_2, resulting in a gas loss and a reduction in deliverability (Reitenbach et al. 2015). Notably, the higher diffusivity of H_2 compared to CH_4 can increase gas loss into the formation water of the cap rock or adjacent aquifer (Carden and Paterson 1979; Krooss 2008).

However, the primary impact of gas diffusion through pore fluids in caprock, reservoir rock, or wellbore cement—particularly in the context of H_2 and CO_2 storage—is the initiation of biochemical and geochemical reactions with substantial consequences. Specifically, mineral dissolution within caprock and wellbore cement can create migration pathways, potentially compromising the integrity of the storage system (Aftab et al. 2023; Fleury et al. 2009; Wigand et al. 2009; Zivar et al. 2021). The primary concern with wellbore cement is that fluid–rock interactions may lead to leakage along the rock–cement and casing–cement interfaces (Gherardi et al. 2012; Labus and Wertz 2017). In reservoir rocks, mineral dissolution or precipitation can alter transport and storage as well as mechanical properties (Dabbaghi et al. 2024; Muller et al. 2024). In the case of CO_2 storage, water–rock interactions primarily result from chemical changes in the brine, such as a reduction in pH due to CO_2 dissolution (Jun et al. 2013). For underground hydrogen storage (UHS), abiotic reactions occur as hydrogen interacts with dissolved ions, such as sulfate in formation water, or with minerals in the rock matrix, including iron-, sulfur-, and carbonate-bearing minerals (Berta et al. 2018; Hassanpouryouzband et al. 2022; Reitenbach et al. 2015). Furthermore, biotic reactions can lead to the permanent conversion of hydrogen into other products, including methane, hydrogen sulfide, and acetic acid (Dopffel et al. 2021; Heinemann et al. 2021). Biotic processes are particularly likely within reservoir rocks, as most microorganisms have cell sizes around 2 μm (Volland et al. 2022). Furthermore, small microorganisms with cell volumes below 0.1 μm^3 (corresponding to a cell size of approximately 0.6 μm, assuming a spherical shape) are often present in aqueous environments (Lauro et al. 2009), indicating that microbial activity could also drive reactions within caprocks, with the majority of pores smaller than 2 μm.

Moreover, hydrogen is generated near radioactive waste repositories through corrosion and radiolysis mechanisms. It partially dissolves in the formation water and dissipates from the repositories by diffusion (Harrington et al. 2012; Ortiz et al. 2002). However, if the gas generation rate exceeds the diffusive flux, a gas pressure buildup and subsequent capillary breakthrough could ultimately compromise the host rock's barrier function (Amann-Hildenbrand et al. 2015; Jacops 2018). Numerous studies have extensively examined diffusion coefficients of various gases, including CH_4, CO_2, and hydrocarbons in liquid or liquid-saturated rocks (Krooss and Schaefer 1987; Pomeroy et al. 1933; Riazi 1996; Upreti and Mehrotra 2000; Zarghami et al. 2017). These investigations have primarily been conducted in the context of underground natural gas storage, CO_2 sequestration, or enhanced oil recovery. Research on effective H_2 diffusivity is still limited, with only a few experimental attempts carried out on liquid-saturated rocks. For instance, the effective H_2 diffusivity was assessed in water-saturated samples of Bentheim sandstone, Werra rock salt, and Opalinus Clay, yielding values in the order of 10^{-9} m^2/s (Strauch et al. 2023). Jacops et al. (2015) performed a study to evaluate the H_2 diffusivity in water-saturated Boom Clay, with the aim of achieving a comprehensive understanding of the balance between gas generation and gas dissipation during the disposal of radioactive waste. The measured values for samples aligned parallel to the bedding were higher than those perpendicular to the bedding, both quantified in the order of 10^{-10} m^2/s. In another experimental study, Michelsen et al. (2022) quantified H_2 diffusivity in water-saturated rock specimens to assess the potential for H_2 loss through cap rocks during UHS. The determined effective diffusivities were in the order of 10^{-11} m^2/s. Despite these efforts, systematic studies on diffusion coefficients of different gases in liquid or through various rocks with varying petrophysical properties are still limited. Jacops et al. (2017) determined diffusion coefficients of dissolved gases of differently sized molecules (He, Ne, H_2, Ar, CH_4, C_2H_6, and Xe) in water and water-saturated clayey and silty Boom Clay. The study investigated the influence of the molecular size of the diffusing species, anisotropy, and pore network geometry on diffusive transport. The diffusion coefficients, in both water and Boom Clay, were found to be inversely related to the kinetic diameter of gases. Furthermore, the study observed that variations in grain size, which significantly affect hydraulic conductivity, resulted in only minor changes in the diffusion coefficients.

In the experimental studies addressing gas diffusivity, the amount of gas that diffuses into liquid is determined by either direct or indirect techniques. Direct methods measure the diffusion coefficient by analyzing changes in the composition of the diffusing species along the length of the sample over time, providing a spatial gradient of concentration (Ratnakar and Dindoruk 2015; Schmidt 1989). Direct diffusion experiments can be performed in various ways. One approach involves gas transport through a water-saturated rock, with gas concentrations measured in the aqueous phase (Hanebeck 1995; Jacops et al. 2013; Schlömer and Krooss 1997). In another approach, gas reservoirs are in direct contact with the water-saturated rock, and concentrations are measured directly from the gas phase using gas chromatography (GC), mass spectrometry (MS) (Hogeweg et al. 2024; Michelsen et al. 2023) or a hydrogen sensor (Strauch et al. 2023). These different approaches may lead to discrepancies in the measured diffusion coefficients. Strauch et al. (2023) determined the hydrogen diffusivity in Opalinus Clay under in situ saturation using the latter approach, finding value 1–2 orders of magnitude higher than those obtained by (Krooss 2008) and (Jacops et al. 2017) through the former approach. This discrepancy can be attributed to the use of gaseous hydrogen instead of dissolved hydrogen, potentially leading to partial drying of the pore system. However, these techniques tend to be expensive and time-consuming as they require compositional analysis

using techniques such as mass spectrometry or chromatography. In contrast, indirect techniques measure changes in physical properties of the gas–liquid system rather than gas concentration (Riazi 1996). Indirect techniques typically rely on measuring various physical properties such as gas pressure (Ratnakar and Dindoruk 2015; Schmidt 1989; Upreti and Mehrotra 2002), volume of dissolved gas (Jamialahmadi et al. 2006; Renner 1988), interface velocity (Das and Butler 1996; Grogan et al. 1988), or magnetic field strength (Wen and Kantzas 2005). The most popular indirect technique is measuring pressure decay within a constant volume cell at a constant temperature. This technique provides a temporal evolution of gas pressure as gas dissolves in a liquid in a closed system. This evolution is then converted to the amount of diffused species using the equation of state for real gas and subsequently a suitable diffusion model is applied to determine the gas diffusion coefficient.

Several researchers have employed the pressure decay method to investigate gas diffusion in liquid-saturated porous media (Gao et al. 2019; Li et al. 2016, 2006; Lv et al. 2019). In the experiments carried out by Gao et al. (2019), the diffusivity of CO_2 in oil-saturated pore space was determined in the direction parallel to the symmetry axis of the cylindrical test samples (i.e., axial direction). They developed a mathematical model that incorporates both porosity and tortuosity to evaluate CO_2 diffusivity based on pressure recording. The study investigated four different types of artificial rocks with varying permeability values under pressure and temperature conditions ranging from 15 to 30 MPa and 20 to 80 °C, respectively. The results indicated that the model could accurately predict the pressure data and CO_2 diffusivity. Furthermore, it has been shown that the measured effective diffusivities correlate positively with permeability and inversely with tortuosity. Li et al. (2006) suggested an experimental method and derived a mathematical model to measure the diffusion coefficient of CO_2 in brine-saturated Berea and Bentheim rock specimens within a pressure range of 2.4–7.3 MPa. Their experimental approach involved sealing the two end faces of the core and allowing gas to diffuse solely in radial direction. This design increases the diffusion area and enables a larger volume of gas to transfer per time interval, resulting in more representative measurements. The mathematical model predicted the experimentally recorded pressure drop over time with good agreement. However, no correlation has been found for effective diffusivities and other petrophysical properties.

This study aims to address the knowledge gap concerning the diffusion coefficients of various gases, particularly hydrogen, in water-saturated rocks using the pressure decay technique. Experiments were conducted on four porous sandstones from Lower Cretaceous (Bentheim and Oberkirchner) and Triassic (Grey and Red Weser) formations, which are reservoir analogues for underground gas storage. Furthermore, the study demonstrates the effectiveness of the pressure decay technique in determining the diffusion coefficients of various gases in both water and water-saturated rocks.

2 Theoretical Background

2.1 Mathematical Model to Determine the Diffusion Coefficient in Water

The analytical model for determining the gas diffusion coefficient in water, as proposed by Ratnakar and Dindoruk (2015), is as follows:

$$\rho_g(t) - \rho_{g\infty} = \beta \exp(\gamma t), \beta = \frac{2\rho_{g0}}{\left(1 + \alpha H_{cc} + \frac{\lambda_1^2}{\alpha H_{cc}}\right)}, \text{ and } \gamma = \frac{-\lambda_1^2 D}{h_L^2} \tag{1}$$

Here, subscripts ∞ and 0 denote the equilibrium and initial conditions for gas density [kg/m^3], respectively, β is the rate coefficient of pressure decay representing the driving force behind the dissolution process [kg/m^3], and γ refers to the exponent factor indicating the rate of pressure decay at late times [1/s]. The other parameters include H_{cc}, representing Henry's constant at a constant temperature [−], α, the volume ratio of the liquid phase to gas phase, h_L, the height of water in the diffusion cell [m], and D, the gas diffusion coefficient [m^2/s], and λ_1 can be approximated by the following equation:

$$\lambda_1 \to \frac{\pi}{2} + \frac{2}{\pi}\alpha H_{\text{cc}} \text{ with } \alpha H_{\text{cc}} \ll 1 \tag{2}$$

The assumptions and derivation process are explained in detail in Appendix A.1

2.2 Mathematical Model to Determine the Effective Diffusion Coefficient in Water-Saturated Rock

According to Li et al. (2006), the effective gas diffusion coefficient in water-saturated rocks during radial gas diffusion can be calculated using the following equation:

$$\Delta P_g = \frac{\text{ZRTN}_\infty}{V_g}\left(1 - \sum_{n=1}^{\infty} \frac{4}{r_0^2 \alpha_n^2} \exp\left(-D_{\text{eff}} \alpha_n^2 t\right)\right) \tag{3}$$

where ΔP_g refers to the pressure drop [Pa] at time t [s], V_g denotes the gas phase volume (i.e., the sum of the reference cell and the diffusion volumes, excluding the bulk volume of the rock specimen) [m^3], Z is the gas compressibility, R is the universal gas constant [8.314 J/(mol·K)], T is temperature [K], N_∞ is the maximum amount of gas that will eventually diffuse into water [mol], D_{eff} is the effective diffusion coefficient [m^2/s], and α_n are the positive roots of the first kind of Bessel function of zero order as follows:

$$J_0(r\alpha_n) = 0 \tag{4}$$

Li et al. (2006) approximated Eq. 3 as a linear relationship between ΔP_g and $\sqrt{t}$, with the slope of k_1, providing an initial estimate for D_{eff}

$$\Delta P_g = k_1 \sqrt{t} \tag{5}$$

with

$$k_1 = \frac{4\text{ZRTN}_\infty}{r_0 V_g}\sqrt{\frac{D_{\text{eff}}}{\pi}} \tag{6}$$

Appendix A.2 provides a detailed explanation of the assumptions and derivation process.

The effective gas diffusion coefficient in a water-saturated rock is a function of the corresponding gas diffusivity in water and the restrictive effects of the microstructure. These effects are attributed to porosity (∅), tortuosity (τ), and constrictivity (δ). Porosity represents

the reduction in available surface area for diffusion, tortuosity describes the deviation of diffusion pathways from a straight pathway, and constrictivity introduces transport resistance that inversely relates to the width of bottlenecks. Constrictivity depends on the ratio of the diffusing molecular diameter to the pore diameter. Thus, the relationship between the effective diffusivity and its corresponding value in water is expressed as follows (Grathwohl 1998):

$$D_{\text{eff}} = D\varnothing\delta/\tau \tag{7}$$

Constrictivity becomes relevant when the size of the species approaches that of the pore (Shen and Chen 2007); however, for pores larger than 1 nm, its value is approximately 1 (Grathwohl 1998). In addition, in most experimental studies, its effect was implicitly included in tortuosity due to the lack of a suitable measurement techniques (Holzer et al. 2013). Furthermore, the diffusive flux in porous media is expressed in two ways in the literature (Bear 1972; Cussler 1997; Krooss et al. 1992; Liu et al. 2012). It can be determined by measuring gas concentration gradients either within the bulk volume (C_r) or within the pore volume (C). The diffusion coefficients obtained from these approaches are related as follow (Li et al. 2006):

$$D^r_{\text{eff}} = \varnothing D^p_{\text{eff}} \tag{8}$$

where D^r_{eff} represents the diffusion coefficient determined based on C_r, while D^p_{eff} corresponds to the diffusion coefficient derived from C. Since porosity is already accounted for in the definition of D^r_{eff}, Eq. 7 is simplified as follows, assuming a constrictivity factor 1 (Li et al. 2006):

$$D^r_{\text{eff}} = D/\tau \tag{9}$$

3 Materials and Methods

3.1 Samples

This study investigated core samples obtained from four distinct sandstone formations, chosen as analogs for underground gas storage reservoirs, characterized by a wide range of permeabilities from 10^{-12} to 10^{-17} m^2 (Arekhov et al. 2023; Nolte et al. 2021; Peksa et al. 2015). Cylindrical plugs (diameter $\approx$14.85 mm; length $\approx$34.8 mm) were drilled from outcrop blocks. The sandstone formations investigated include the Lower Cretaceous (Valanginian) Bentheim sandstone from the westernmost Lower Saxony Basin, Germany, the Triassic (Olenekian) Grey (GWS) and Red Weser sandstone (RWS) from the Lower Solling Formation of the Reinhardswald Basin, Germany, and the Lower Cretaceous (Berriasian) Oberkirchner (OBK) sandstone from the Lower Saxony Basin, Germany. Comprehensive descriptions of these rock specimens are documented in Khajooie et al. (2024b).

3.2 Experimental Setup and Procedure

3.2.1 Setup

Gas diffusion coefficients in water and water-saturated rocks were determined in two similar setups: one with three high-pressure diffusion cells (Fig. 1) and another with a

single cell. Each cylindrical diffusion cell (V_{sc} = 19.5 to 27.7 mL) was equipped with a welded Keller pressure transducer with a precision of ± 0.1 kPa (± 0.01% of the full scale range: 1.0 MPa) and a capillary connected to a multi-positioning selector valve (Valco). The diffusion cells were sealed with stainless steel porous filters (*FITOK Snubber gasket with silver coating for additional sealing*) and intermittently linked to the selector valve ports, with a port in between for a closed position. The selector valve was also connected to a reference cell (V_{ref} = 83.9 mL), which ensured that the pressurized gas reached the equilibrium temperature before expansion to the diffusion cells. Valves 1 and 2 were installed before the reference cell to connect the system to different gas bottles (He, H_2, Ar, CO_2, and CH_4) for pressurizing, or a vacuum pump for evacuation. In our setup, O-rings were deliberately excluded to prevent any interaction between gas molecules and rubber or FKM (Viton) seals, which could cause swelling. The entire system was placed in an oven, and the temperature was maintained at 35 ± 0.1 °C (Fig. 1). The temperatures of the diffusion cells and the reference cell were measured using their corresponding transducers directly connected to them. Prior to diffusion measurements, a leak test with helium was performed on all reference and diffusion cells at a pressure of 1.0 MPa with recorded leak rates ranging from 0.001 to 0.01 kPa/h. The pressure stability of the system revealed that temperature fluctuations had a negligible effect on the pressure within ± 0.1 kPa for a period of 10 h. Furthermore, the volume calibration of reference and diffusion cells as well as their corresponding pressure transducers and capillaries was performed by the expansion of helium into the system from a known volume. The maximum pressure applied for calibration was 1.0 MPa, and the coefficient of variations of the measured volumes ranged from 0.08 to 0.46%. The blank experiments (detailed in Appendix A3) were conducted on all cells with helium to establish the baseline for pressure transducer recordings.

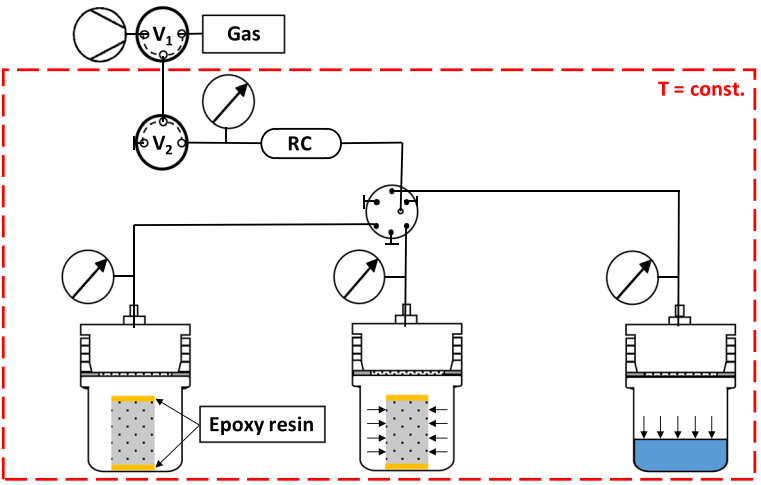

Fig. 1 Experimental setup for measuring gas diffusion in water and water-saturated rock specimens using the pressure decay method. The top and bottom end faces of the rock specimens were sealed with epoxy resin (yellow color) to enable gas diffusion exclusively in the radial direction (as denoted by the horizontal arrows) through the porous column. Gas diffusion tests in water were conducted vertically (as indicated by the vertical arrows), from top to bottom

3.2.2 Deionized Degassed Water

The water used in the diffusion experiments was deionized and degassed. Degassing was achieved by evacuating the water samples in a desiccator for 24 h.

3.2.3 Gas Diffusion Experiments in Water

To measure the diffusion coefficient of gases in water, approximately 10 mL of water was added to each cell. Then, the reference cell and a diffusion cell, along with their respective capillaries and pressure transducers, were evacuated. Subsequently, the reference cell was pressurized with either H_2, He, CH_4, Ar, or CO_2 to a desired pressure and allowed to temperature-equilibrate for 2 h. The respective gas was then expanded into the diffusion cell, after which the cell was closed. Next, the pressure decay within the cell was continuously monitored. Similar procedures were repeated to conduct diffusion experiments in other cells. The diffusivities of all aforementioned gases in water were measured at 1.0 MPa.

3.2.4 Setup Validation

The validation of the setup was assessed by conducting repeatability tests with H_2 and CH_4 in water, each in a separate diffusion cell at 0.5 and 0.2 MPa, respectively. Furthermore, setup independency was tested by parallel measurements in different cells using the same gas and maintaining consistent boundary conditions. Hereby, CH_4 diffusivities in water were determined simultaneously in four cells at a pressure of 1.0 MPa. These findings were compared with corresponding values reported in the literature under similar boundary conditions. Furthermore, a repeatability test was conducted on the water-saturated Bentheim rock specimen to determine the effective diffusivity of H_2 at a pressure of 1.0 MPa. The procedures for these experiments are detailed in Chapter 3.2.5.

3.2.5 Gas Diffusion Experiments in Water-Saturated Rock Specimens

The rock specimens were prepared for experiments by sealing their two end faces using epoxy resin (*Araldite XW396*), allowing it to solidify over a 24-h period. The dry rock specimens were weighed and immersed in water within an evacuated desiccator to achieve full saturation. To verify full saturation, the weight difference before and after saturation was compared to the pore volumes measured using He-pycnometry and water immersion porosimetry techniques. Upon completion of the preparation process, the saturated rock specimens were positioned within the cells, and the diffusion experiments were carried out following the procedures detailed in Chapter 3.2.3. These experiments were conducted under a pressure of 1.0 MPa to ascertain the diffusivity of H_2, CH_4, and CO_2 within individual water-saturated rock specimens.

3.3 Pore Volume Measurement

The pore volume of cylindrical rock specimens was determined through He-pycnometry and water immersion porosimetry methods. These techniques are well-documented in

the literature, offering comprehensive explanations of the equipment and methodology employed (Gaus et al. 2019; Hu et al. 2021).

4 Results and Discussion

4.1 Determination of Gas Diffusion Coefficients in Water

The measured pressures during a CH_4 diffusion test in water ($P = 1.0$ MPa; $T = 35$ °C) were evaluated with the mathematical model outlined in Chapter 2.1 to determine the diffusion coefficient. Gas densities were calculated from the recorded pressures and temperatures using the GERG-2008 equation of state (Kunz and Wagner 2012) and subsequently plotted against time (Fig. 2a). As the experiment continued until pressure equilibrium was reached, the final equilibrated density ($\rho_{g\infty}$) was obtained by averaging the density readings at this phase (after 200 h), resulting in a value of 6.084 kg/m^3. To linearize the data, $\ln\left(\rho_g(t) - \rho_{g\infty}\right)$ was plotted against time, facilitating the preliminary determination of γ and β, which were found to be 0.022 1/h and 0.192 (exp(−1.65)) kg/m^3, respectively, as derived from the slope and intercept (Fig. 2b). These parameters were subsequently fine-tuned employing an optimization algorithm to align the model with experimental observations. The optimized values for γ and β were determined to be 0.021 1/h and 0.188 kg/m^3, respectively. Ultimately, the gas diffusion coefficient was determined using Eq. 1, by with γ, λ_1 (1.6) and h_L (0.033 m) known, resulting in a value of $2.59 \cdot 10^{-9}$ m^2/s.

4.2 Determination of Gas Diffusion Coefficients in Water-Saturated Rock Specimens

The pressure decay recorded during the CH_4 diffusion experiment on water-saturated OBK (Fig. 3a) was analyzed by the mathematical model presented in Chapter 2.2. This evaluation was performed after subtracting the pressure drop observed during the blank experiments,

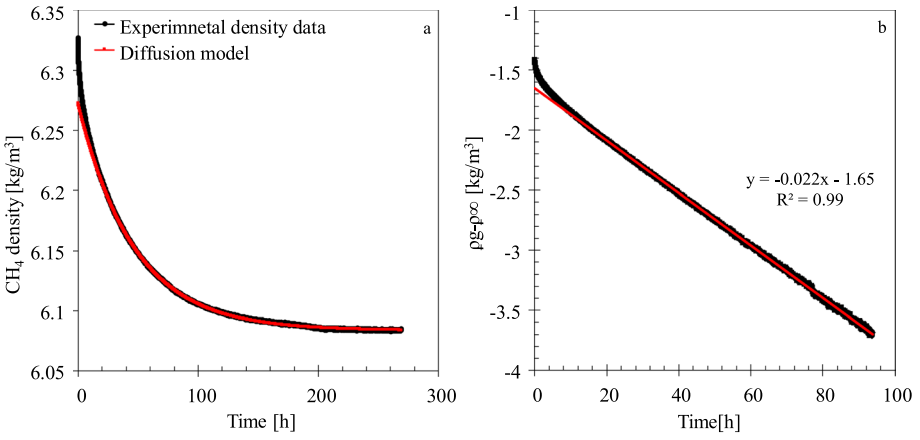

Fig. 2 Comparison of the density derived from pressure decay measured during CH_4 diffusion in water with the model after regression **a**, semi-log plot of $\left(\rho_g(t) - \rho_{g\infty}\right)$ against time, representing the driving force for gas dissolution, to derive the γ and β values as the slope and intercept of the plots, respectively **b**

in order to eliminate the impact of this artifact (see Appendix A.3). The experiment was carried out at a pressure of 1.14 MPa and a temperature of 35 °C. The pressure drop (ΔP) was calculated and plotted against the square root of time, revealing four distinct zones characterized by their slopes (Fig. 3b). In the initial stage, marked in blue, pressure decline occurs more rapidly than in the subsequent linear phase (Fig. 3b). This deviation, similarly observed in other diffusion studies, was dismissed, as the subsequent linear portion holds greater relevance in determining the diffusion coefficient (Caskey et al. 1973; Reamer et al. 1956; Renner 1988; Tan and Thorpe 1992). The observed positive intercept primarily arises from the dissolution of gas into the water film surrounding the outer surface of the rock specimen, thereby establishing a stable gas concentration at the gas–water interface. Consequently, this period is commonly referred to as the "incubation region" (Renner 1988). While fluctuations in temperature and pressure resulting from gas expansion into the diffusion cell may play a role during this phase, their influence is minor in comparison to gas dissolution (Li et al. 2016, 2006). The linear phase (yellow zone), known as the steady-state diffusion stage (Caskey et al. 1973; Reamer et al. 1956; Renner 1988; Tan and Thorpe 1992), represents transfer of gas molecules from the gas–liquid interface toward the center of rock specimens. Subsequently, the plot of ΔP versus $\sqrt{t}$ begins to deviate from linearity, leading to a transition (green zone), which indicates that gas molecules have reached the center of the rock specimens. This suggests that the assumption of the semi-infinite diffusion pathway is no longer applicable (Renner 1988). However, this assumption remains valid and introduces minimal uncertainties in interpreting the data, provided that the liquid phase contains less than half the gas necessary for full saturation (Pomeroy et al. 1933). Finally, when the gas concentration within the water-saturated rock specimen becomes equal to that on the outer surface, thereby eliminating concentration gradients, the stabilized phase (orange zone) occurs.

An initial approximation of the diffusivity was derived by applying Eq. 6, yielding a value of $2.32 \cdot 10^{-9}$ m^2/s. This was obtained from the slope of the linear relationship between

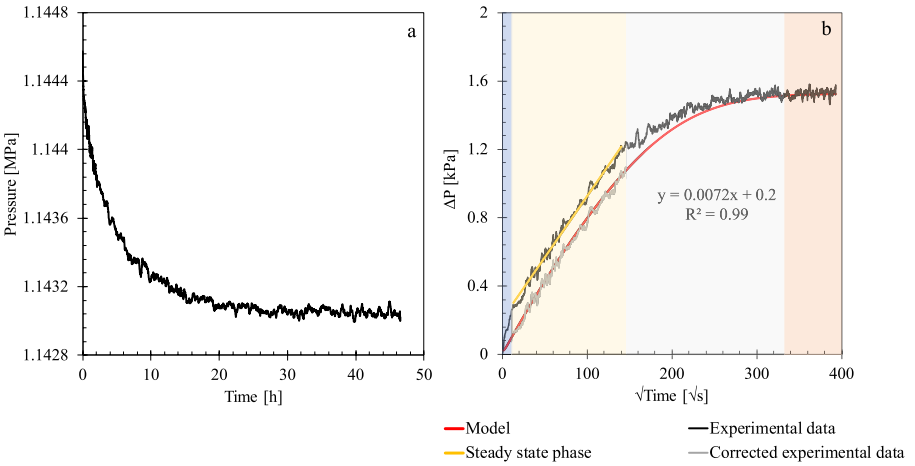

Fig. 3 **a** Pressure decay observed during the CH_4 diffusion experiment on water-saturated OBK over time and **b** comparison between the corrected experimental ΔP plotted against the square root of time ($\sqrt{t}$) with the ΔP derived from the mathematical model. The experimental ΔP plot delineates four distinct zones: the incubation (blue shading), the steady-state diffusion (yellow shading), the transition (green shading), and stabilized stages (orange shading)

ΔP and $\sqrt{t}$ during the steady-state diffusion phase. Subsequently, the initial mathematical model was developed, allowing for the quantification of the additional ΔP during the incubation stage by calculating the average deviation between the model and experimental data. This enabled correction of the experimental dataset. The effective gas diffusivity was then accurately determined by fitting the mathematical model to the corrected experimental data in this phase (Fig. 3b), resulting in an adjusted value of $3.7{\cdot}10^{-9}$ m^2/s. As depicted in the plot, the theoretical ΔP intersects the origin, whereas extrapolating the straight part of experimental data to $\sqrt{t}=0$ yields a positive intercept, indicative of a deviation in the incubation phase.

The analysis of steady-state diffusion stage across all measurements indicates that this phase maintains linearity until the total quantity of diffused gas reaches between 50 and 75% of the saturation limit. Therefore, when the recorded gas uptakes achieve 50% of full saturation, assuming the setup is leak-tight, the experimental results can be confidently evaluated. This is because only the linear portion of the plot is relevant for determining the diffusion coefficient. The influence of leak rate on experimental outcomes has been examined, revealing that the measurements remain unaffected by leak rates on the order of 10^{-2} kPa/h.

4.3 Data Validity and Accuracy

A series of experiments were conducted to thoroughly evaluate the reliability and accuracy of the setup. This involved reproducing the diffusion coefficients of H_2 and CH_4 in water as reported by Jähne et al. (1987), which were $6.2{\cdot}10^{-9}$ and $2.4{\cdot}10^{-9}$ m^2/s, respectively. These values were determined by measuring the gas concentration at a pressure of 0.1 MPa and a temperature of 35 °C without applying any pressure gradient. Jähne et al. (1987) reported a maximum systematic error of 5% or less. To validate our findings, five repeatability tests of H_2 and CH_4 diffusivities in water have been conducted using a specific cell for each gas, under pressure of 0.5 and 0.2 MPa ($T=35$ °C), respectively. The results of these experiments are illustrated in Fig. 4a. The observed diffusion coefficients of H_2 and CH_4 in water ranged from $6.3{\cdot}10^{-9}$ to $7.0{\cdot}10^{-9}$ m^2/s and $2.3{\cdot}10^{-9}$ to $2.9{\cdot}10^{-9}$ m^2/s, respectively, with corresponding standard deviations of $0.3{\cdot}10^{-9}$ and $0.3{\cdot}10^{-9}$ m^2/s, indicative of the reproducibility of our measurements. Furthermore, the average measured diffusivities for H_2 and CH_4 were $6.7{\cdot}10^{-9}$ and $2.7{\cdot}10^{-9}$ m^2/s, respectively, showing a minor deviation of 5.1% and 6.8% from literature values, emphasizing good agreement. Furthermore, a comparability assessment was conducted to evaluate the findings derived from four diffusion cells within the experimental setup. This entailed measuring the diffusivity of CH_4 in water across four cells, under consistent boundary conditions of 1.0 MPa pressure and 35 °C temperature. As depicted in Fig. 4a, the measured diffusion coefficients ranged from $2.6{\cdot}10^{-9}$ to $3.1{\cdot}10^{-9}$ m^2/s, with the standard deviation of $0.2{\cdot}10^{-9}$ m^2/s, indicating consistent experimental findings regardless of the specific diffusion cell used. It is worth noting that the experiments were conducted at higher pressures than those reported in the literature to enhance the accuracy of measurements. It was observed that experiments performed at lower pressures experienced significant pressure fluctuations, likely due to minor temperature variations, which impeded the accurate determination of diffusivity. Additionally, the effect of pressure on the diffusion coefficient is negligible, as discussed in detail in Chapter 4.4.

Moreover, to evaluate the accuracy and reliability of gas diffusivity measurements in water-saturated rocks, five experiments were conducted to reproduce the diffusion of H_2

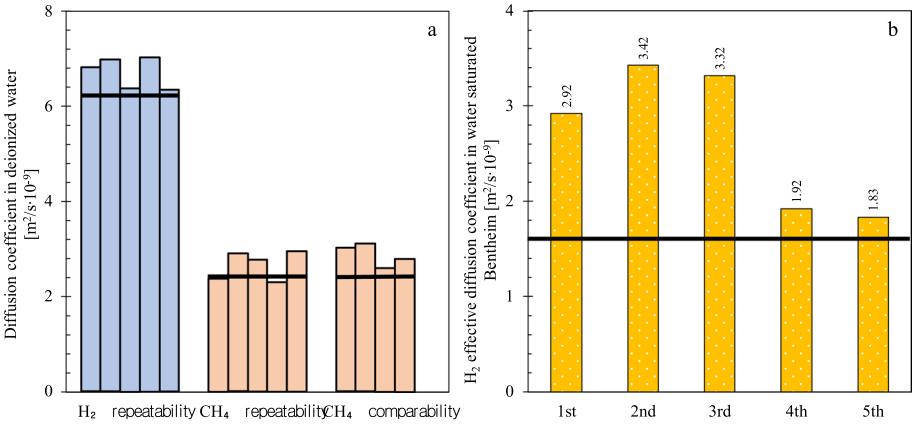

Fig. 4 **a** The diffusion coefficients of H_2 and CH_4 in water, as determined in repeatability and comparability tests, were compared with corresponding literature data (Jähne et al. 1987). The repeatability tests for H_2 and CH_4 were conducted at pressures of 0.02 MPa and 0.05 MPa, respectively. The comparability tests involved comparing results obtained from different diffusion cell. These experiments, which measured CH_4 diffusivity in water across four cells, were performed at a pressure of 1.0 MPa. All tests were conducted at a temperature of 35 °C. **b** Comparison of five measurements of the H_2 effective diffusion coefficient in water-saturated Bentheim sandstone ($P = 1.0$ MPa; $T = 35$ °C) against literature value (Strauch et al. 2023)

in water-saturated Bentheim. A comparative analysis was then performed against existing literature (Fig. 4b). Diffusivity values for H_2 measured in this study ranged between $1.9{\cdot}10^{-9}$ and $3.4{\cdot}10^{-9}$ m^2/s, with an average of $2.9{\cdot}10^{-9}$ m^2/s and a standard deviation of $0.6{\cdot}10^{-9}$ m^2/s. The consistently low standard deviations indicate a sufficient reproducibility of diffusion measurements within water-saturated rocks. Furthermore, H_2 diffusivity in water-saturated Bentheim utilizing a direct method (Strauch et al. 2023) was similar at $1.6{\cdot}10^{-9}$ m^2/s.

4.4 Diffusion of Gases in Water

The diffusion coefficients of H_2, He, CH_4, Ar, and CO_2 were precisely determined under consistent boundary conditions of 1.0 MPa and 35 °C. The findings from these experiments, as well as those from reproducibility and comparability assessments detailed in Chapter 4.3, are presented in Table 1 and depicted in Fig. 5. The mean diffusivities for H_2 and CH_4 are $6.7{\cdot}10^{-9}$ and $2.8{\cdot}10^{-9}$ m^2/s, respectively, with standard deviations of $0.3{\cdot}10^{-9}$ for both gases. The observed diffusivity values for He, Ar, and CO_2 in water are $9.6{\cdot}10^{-9}$, $10.9{\cdot}10^{-9}$, and $44.56{\cdot}10^{-9}$ m^2/s, respectively.

The diffusion coefficients of the gases under examination in water were already determined through a range of direct methods including Raman spectroscopy (Chen et al. 2018; Guo et al. 2013), capillary cell (Sahores and Witherspoon 1970; Witherspoon and Saraf 1965), diaphragm cell (Gubbins et al. 1966; Vivian and King 1964), modified Barrer (Jähne et al. 1987), and Taylor dispersion (Cadogan et al. 2014; Frank et al. 1996) across various pressures and temperatures, often differing from those employed in our research. All these techniques determine the diffusion coefficient by analyzing the gas concentration in the liquid phase. At a given pressure, increasing the temperature leads to higher diffusion coefficients. This behavior likely arises from the increased kinetic energy of gas and water molecules, as well as a

Table 1 Overview of the measured diffusion coefficients of H_2, H_2, CH_4, Ar, and CO_2 in water under indicated pressures and 35 °C

Gas	Pressure [MPa]	Temperature [°C]	Diffusion coefficient [10^{-9} m^2/s]
H_2	0.5	35.0	6.8
	0.5	35.0	7.0
	0.5	35.0	6.4
	0.5	35.0	7.0
	0.5	34.9	6.3
CH_4	0.2	36.6	2.4
	0.2	36.6	2.9
	0.2	36.6	2.8
	0.2	36.6	2.3
	0.2	36.6	2.9
	1.0	36.6	3.0
	1.0	34.9	3.1
	1.0	36.2	2.6
	1.0	34.8	2.8
He	0.9	36.6	9.6
Ar	1.0	36.6	10.9
CO_2	1.0	34.9	44.6

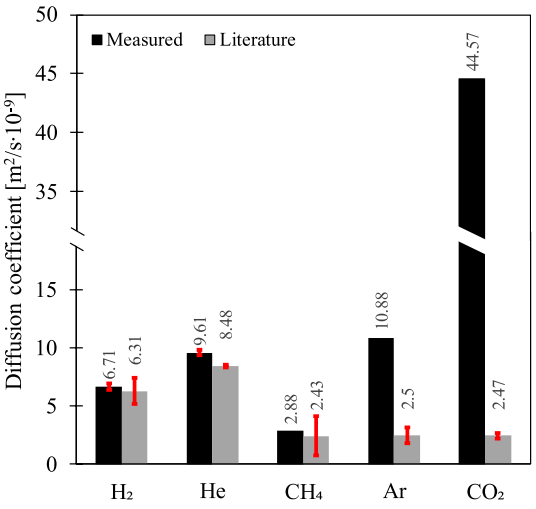

Fig. 5 Comparison of measured diffusivities of H_2, He, CH_4, Ar, and CO_2 with their respective average values from the literature compiled in Table 2. The H_2 and CH_4 diffusivities were determined by averaging the results presented Chapter 4.3. While the diffusion coefficients of H_2, He, and CH_4 closely align with their published values, significant disparities are evident for Ar and CO_2 when compared to their corresponding literature data. Red bars indicate standard deviations

reduction in water viscosity, which facilitates diffusive mass transport (Upreti and Mehrotra 2002). The Stokes–Einstein relation describes this temperature dependence, indicating that the product of the diffusion coefficient and viscosity is directly proportional to temperature (Guo et al. 2013):

$$D = \frac{k_B(T + 273.15)}{6\pi\mu r_s} \tag{10}$$

where k_B is the Boltzmann constant [$1.38 \cdot 10^{-23}$ J/K], T is temperature [℃], μ represents viscosity of water, and r_s [nm] is the radius of the diffusing solute molecule. Assuming r_s remains constant with temperature, the diffusion coefficient at desired temperature (T_2 =35 °C) can be determined from its corresponding value at T_1 using known water viscosities at these temperatures (Li 2006):

$$D_{T_2} = \frac{D_{T_1} \mu_{T_1} \left(T_2 + 273.15\right)}{\left(T_1 + 273.15\right) \mu_{T_2}} \tag{11}$$

Conversely, several researchers have reported that the impact of pressure on gas diffusivities in water is negligible. Guo et al. (2013) conducted an investigation into the diffusion coefficients of CH_4 in water across a range of pressures from 5 to 40 MPa. Their investigation revealed a minor discrepancy of only 3% between the lowest and highest measured values (Table 2). In another study, Sachs (1998) examined CH_4 diffusivities in water within a pressure range of 7.6–32.5 MPa, maintaining a constant temperature of 50 °C. While this study suggested the potential impact of pressure on diffusion coefficients, it is found that within the specified pressure range, CH_4 diffusivities varied from $3.6 \cdot 10^{-9}$ to $3.2 \cdot 10^{-9}$ m^2/s. Furthermore, two experimental studies were carried out to explore the diffusion behavior of CO_2 in water across a pressure range of 10 MPa to 45 MPa. Similarly, these investigations inferred that the impact of pressure on CO_2 diffusion coefficients in water remained minimal within the examined ranges (Cadogan et al. 2014; Lu et al. 2013). However, research conducted by Renner (1988) on CO_2 diffusivity in 0.25M NaCl brine at a temperature of 38 °C, across a pressure range of 1.5–5.8 MPa, revealed an upward trend in diffusivity with increasing pressure. The latter investigation has been performed through the monitoring of volume changes over time under constant pressure. The observed diffusivities ranged from $3.0 \cdot 10^{-9}$ to $7.3 \cdot 10^{-9}$ m^2/s across the examined pressure range, surpassing those previously documented in the literature (Table 2).

Diffusion coefficients for H_2, He, CH_4, Ar, and CO_2 derived from literature (Table 2) were averaged, resulting in values of $6.2 \cdot 10^{-9}$, $8.3 \cdot 10^{-9}$, $2.1 \cdot 10^{-9}$, $2.5 \cdot 10^{-9}$, and $2.4 \cdot 10^{-9}$ m^2/s, respectively, with corresponding standard deviations of $1.1 \cdot 10^{-9}$, $1.7 \cdot 10^{-9}$, $0.1 \cdot 10^{-9}$, $0.7 \cdot 10^{-9}$, and $0.2 \cdot 10^{-9}$ m^2/s. These values are in good agreement with our experimentally obtained diffusion coefficients, particularly for H_2, CH_4, and He (Fig. 5). However, the observed diffusivity values for Ar and CO_2 in water demonstrate significant discrepancies compared to the literature data. Measured diffusion coefficients for Ar and CO_2 amount to $10.9 \cdot 10^{-9}$ and $44.6 \cdot 10^{-9}$ m^2/s, respectively, representing one order of magnitude higher than their corresponding literature values. This significant discrepancy can be attributed to the formation of a denser layer at the gas–liquid interface, caused by dissolution of the CO_2 and Ar molecules. The change in water density is governed by the concentration of gas in water and the molar mass-to-molar volume ratio of the dissolved gas molecules. Previous experimental and modeling studies have shown that CO_2 and Ar dissolution increases water density, while CH_4 dissolution leads to a decrease (Duan and Mao 2006; Watanabe and Iizuka 1985). This occurs because the molar volume of any gas dissolved in water is greater than that of pure water; thus, the dissolution of CH_4, with a molar mass of 16 g/mol—lower than that of water (18 g/mol)—results in a reduction in density. Consequently, the measured CH_4 diffusivity in water remains unaffected by density-driven convection, despite its solubility being similar to that of Ar (Sander 2015).

The denser water layer formed by CO_2 and Ar establishes a distinct density gradient within the water column, thereby triggering convective transport phenomena. With convective transport exerting a dominant influence, the evaluation of pressure decay results in a

Table 2 Compilation of experimental and calculated diffusion coefficients for H_2, H_2, CH_4, Ar, and CO_2 in water, derived from various methodologies under different pressures and temperatures

Gas	Pressure [MPa]	Diffusion coefficient [10^{-9} m^2/s]	Method (reference)	Gas	Pressure [MPa]	Diffusion coefficient [10^{-9} m^2/s]	Method (reference)
CH_4	5	2.1	Raman spectroscopic (Guo et al. 2013)	H_2	0.1	5.1	Diaphragm cell (Gubbins et al. 1966)
	10	2.1			0.1	5.5	Laminar dispersion (Ferrell & Himmelblau 1967)
	20	2.1			0.1	7.6	Bubble collapse (Wise & Houghton 1966)
	30	2.1			0.1	6.1	Diaphragm cell (Vivian & King 1964)
	40	2.1			0.1	6.3	Dissolution of bubbles Hughton (Houghton et al. 1962)
	0.1	2.2	Capillary cell (Sahores & Witherspoon 1970)		0.1	6.8	Wetted sphere (Baird & Davidson 1962)
	0.1	2.1	Capillary cell (Witherspoon & Saraf 1965)		0.1	8.9	Wetted sphere (Davidson 1957)
	0.1	2.3	Diaphragm cell (Gubbins et al. 1966)		0.1	5.2	Rising bubble (Gertz & Loeschcke 1954)
	8.0	2.3	Pressure decay (Sachs 1998)		0.1	5.7	Polarography (Aikazyan & Fedorova 1952)
	0.1	2.0	Moving boundary (Maharajh & Walkley 1973)		0.1	5.1	Gel (Tammann & Jessen 1929)
	0.1	2.4	Modified Barrer (Jähne et al. 1987)		0.1	6.2	Modified Barrer (Jähne et al. 1987)
	10.3	2.0	Raman spectroscopic (Chen et al. 2018)	CO_2	14	2.6	Taylor dispersion (Cadogan et al. 2014)
	0.1	2.1	Theoretical study (Oelkers 1991)		31.6	2.7	Taylor dispersion (Cadogan et al. 2014)
He	0.1	7.6	Laminar dispersion (Ferrell & Himmelblau 1967)		47.7	2.9	Taylor dispersion (Cadogan et al. 2014)
	0.1	7.9	Bubble collapse (Wise & Houghton 1966)		0.1	2.5	Moving boundary (Maharajh & Walkley 1973)
	0.1	8.1	Diaphragm cell (Vivian & King 1964)		0.1	2.4	Modified Barrer (Jähne et al. 1987)
	0.1	8.1	Dissolution of bubbles (Houghton et al. 1962)		0.1	2.5	Taylor-Aris dispersion (Frank et al. 1996)

Table 2 (continued)

Gas	Pressure [MPa]	Diffusion coefficient [10^{-9} m^2/s]	Method (reference)	Gas	Pressure [MPa]	Diffusion coefficient [10^{-9} m^2/s]	Method (reference)
	0.1	12.1	Wetted sphere (Baird & Davidson 1962)		10	2.1	Raman spectroscopic (Lu et al. 2013)
	0.1	6.1	Rising bubble (Gertz & Loeschcke 1954)		20	2.4	
	0.1	8.5	Modified Barrer (Jähne et al. 1987)		30	2.2	
Ar	0.1	1.8	Moving boundary (Maharajh & Walkley 1973)		40	2.0	Volume of dissolved gas (Renner 1988)
	0.1	3.2	Bubble collapse (Wise & Houghton 1966)		1.54	3.1	
					2.92	3.6	
					4.46	4.9	
					5.67	6.7	

To ensure consistency, diffusion coefficients were adjusted to 35 °C using the $D\mu/T$ constant, considering the differing temperature conditions of the original measurements

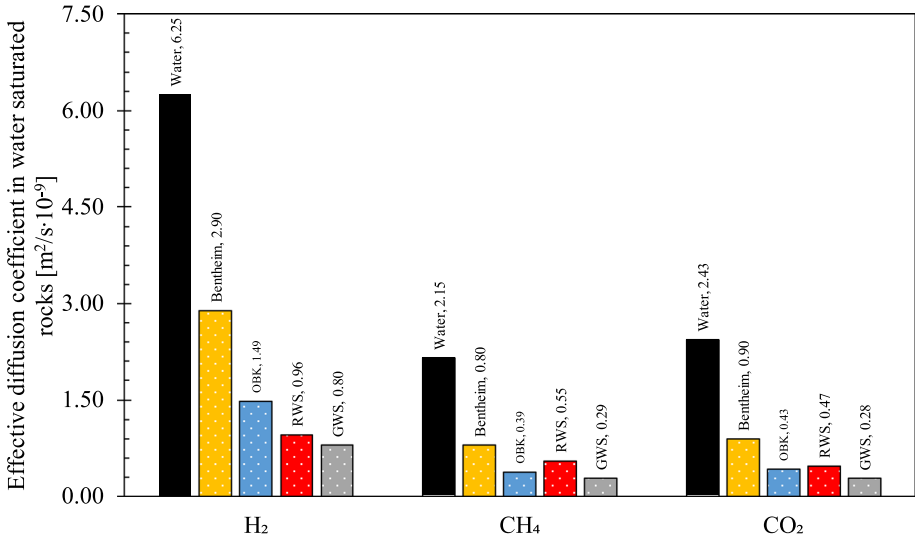

Fig. 6 Comparison of effective diffusivity for H_2, CH_4, and CO_2 within water-saturated specimens of Bentheim, OBK, RWS, and GWS rocks, alongside the corresponding gas diffusion coefficients in water

non-representative diffusivity coefficient (Blair and Quinn 1969; Gholami et al. 2015; Gill et al. 1997). Other researchers, employing the change in gas volume over time at constant pressure to ascertain the diffusivity of Ar in Benzene, have likewise documented this issue. (Bennett et al. 1968).

4.5 Diffusion of Gases into Water-Saturated Rock Specimens

Effective diffusion coefficients of H_2, CH_4, and CO_2 in water-saturated rock specimens from Bentheim, OBK, RWS, and GWS formations were determined and compared with the corresponding diffusion coefficients in water (Fig. 6). The effective H_2 diffusivity ranges from $0.8{\cdot}10^{-9}$ to $2.9{\cdot}10^{-9}$ m^2/s, while the CH_4 and CO_2 effective diffusion coefficients vary from $0.3{\cdot}10^{-9}$ to $0.8{\cdot}10^{-9}$ m^2/s and from $0.2{\cdot}10^{-9}$ to $0.9{\cdot}10^{-9}$ m^2/s, respectively (Table 3). The effective diffusivity of H_2, CH_4, and CO_2 within water-saturated rock specimens investigated in this study has not been previously documented under identical pressure and temperature conditions. Nevertheless, two experimental studies have measured the effective diffusivities of H_2 and CO_2 in the water-saturated Bentheim sandstone, yielding diffusivities of the same order of magnitude: $1.6{\cdot}10^{-9}$ m^2/s for H_2 (Strauch et al. 2023) and $0.5{\cdot}10^{-9}$ m^2/s for CO_2 (Li et al. 2006). The H_2 diffusivity was determined under ambient pressure and temperature by measuring the gas concentration gradient, while the CO_2 diffusivity was determined using the pressure decay method under conditions of 4.4 MPa pressure and 59 °C temperature.

To further characterize the rock specimens, the diffusive tortuosity was calculated using Eq. 9. The majority of pore throat diameters in the examined rock specimens were found to exceed 0.1 µm, while the molecular diameters of H_2, CH_4, and CO_2 are 0.29, 0.38, and 0.33 nm (Gnanasekaran and Reddy 2013), respectively. Given that the ratio of molecular diameter to pore diameter is significantly less than 1, the constrictivity factor for these

Table 3 Overview of the effective diffusion coefficients (D_{eff}) measured and tortuosities calculated for H_2, CH_4, and CO_2 within water-saturated specimens of Bentheim, OBK, RWS, and GWS

Sample	Gas	Average pressure (MPa)	ΔP (kPa)	V (cm^3)	C_0 (10^{-3} mol/cm^3)	Z	D_{eff} (10^{-9} m^2/s)	Tortuosity
Bentheim	H_2	1.016	1.70	15.12	7.39	1.006	2.90	2.2
	CH_4	0.964	15.23	19.28	11.02	0.986	0.80	3.0
	CO_2	1.075	38.43	21.54	291.75	0.950	0.90	2.7
OBK	H_2	1.092	1.35	14.28	7.97	1.006	1.49	4.2
	CH_4	1.144	1.52	21.38	13.49	0.983	0.39	6.3
	CO_2	1.075	29.75	21.38	291.95	0.950	0.43	5.7
RWS	H_2	1.038	1.25	14.02	7.59	0.985	0.96	6.5
	CH_4	1.059	1.93	14.02	12.12	0.984	0.55	4.4
	CO_2	1.086	19.66	21.46	294.94	0.950	0.47	5.3
GWS	H_2	1.037	0.63	13.80	7.59	1.006	0.80	7.7
	CH_4	1.047	0.93	13.80	11.98	0.984	0.29	8.4
	CO_2	1.061	13.89	21.24	288.44	0.951	0.28	8.5

Additionally, the experimental average pressure, ΔP, gas cap volume (V), gas solubility (C_0), and gas compressibility (Z) are provided

gases can thus be reasonably approximated as 1 (Grathwohl 1998; Renkin 1954). Furthermore, the diffusion model for water-saturated rocks used in this study has been developed in analogy to diffusion in bulk liquids (Li et al. 2006), indicating that porosity is incorporated into the diffusion coefficient. Therefore, Eq. 9 is appropriate for relating effective diffusivity to the value measured in water. The obtained values ranged from 2.2 to 3.0 for Bentheim, 4.2 to 6.3 for OBK, 4.4 to 6.5 for RWS, and 7.7 to 8.5 for GWS rock specimens depending on the gas type. As tortuosity increased from 2.6 to 8.1, the effective diffusivities of investigated gases decreased, with reductions ranging between 60 and 80% (Table 3). This suggests that the complex pore network and tortuous pathways substantially interfere with the diffusion process. The diffusive tortuosity for Bentheim sandstone has been previously determined through the measurement of CH_4 effective diffusivities in oil-saturated rock samples (pressure decay method) ranging from 2.7 to 4.1 (Li and Dong 2010). As previously discussed, determining the CO_2 diffusion coefficient in water posed challenges possibly due to the interference of density-induced natural convection. Nevertheless, the similarity observed in the tortuosity derived from CO_2 measurements compared to those of H_2 and CH_4 measurements suggests that the convective transport occurring during CO_2 diffusion in water was effectively impeded. This can be attributed to the presence of the porous medium acting as obstacle, resulting in diffusive transport dominating the process (Gholami et al. 2015). The comparable tortuosity values derived from different gas measurements suggest that CO_2 diffusion coefficients in water can be estimated indirectly. This approach involves measuring the effective CO_2 diffusivity in a rock specimen and utilizing the tortuosity obtained from other gas diffusivity measurements, such as CH_4 or H_2 which are not influenced by density-driven convection (Li and Dong 2010; Li et al. 2006). Thus, employing Eq. 9 allows for the computation of the CO_2 diffusion coefficient in water, resulting in values spanning from $2.3{\cdot}10^{-9}$ to $2.5{\cdot}10^{-9}$ m^2/s, which align well with those documented in the literature (Table 2). Likewise, Li and Dong (2010) conducted calculations of CO_2 diffusion coefficients in water, utilizing tortuosity values acquired from

effective diffusion measurements of CH_4 within Berea and Bentheim sandstones. The outcomes revealed values within the range of $1.9{\cdot}10^{-9}$–$2.7{\cdot}10^{-9}$ m^2/s, consistent with previously reported values (Table 2).

The variation in effective diffusivities of each gas across the studied rock specimens can be attributed to differences in pore structure, which impact the effective area available for gas transport and lead to deviation in diffusion paths from a straight pathway, known as tortuosity (Bear 1972; Grathwohl 1998). This effective area is influenced by the matrix structure and is largely governed by porosity. Furthermore, tortuosity is inversely related to porosity, as supported by numerous studies in the literature (da Silva et al. 2022; Ghanbarian et al. 2013; Holzer et al. 2023). Thus, porosity influences the diffusion mechanism by affecting both the available area at the gas–liquid interface for molecular transport and the complexity of the diffusion pathway. Additionally, as permeability and mean pore diameter are directly related to porosity in sandstones (Chilingar 1964; Nelson 1994; Tiab and Donaldson 2016), their values also offer insights into these diffusion constraints.

The measured effective diffusion coefficients were plotted against porosity, permeability, and mean pore diameter properties, demonstrating positive correlations in Fig. 7a–c. Permeability values of examined rocks were sourced from the literature (Arekhov et al. 2023; Nolte et al. 2021; Peksa et al. 2015), while mean pore diameters were determined from pore throat size distribution obtained through mercury injection capillary pressure measurements, previously published (Khajooie et al. 2024a). RWS was not included for permeability correlation since no permeability measurements for RWS were found in the literature. These correlations (Fig. 7a–c) suggest that the increase in effective gas diffusivity from GWS, RWS, OBK, to Bentheim correspond to an expanded area for gas transport and a reduction in tortuous pathways. Additionally, Fig. 7a reveals a steeper increasing trend for porosity above 15% compared to values below 15%. This observation aligns with the semi-logarithmic relationship of effective diffusion coefficients with permeability and mean pore diameter. Thus, the influence of pore structure in reducing available area for diffusion and imposing tortuous pathways is more pronounced in tight rocks compared to highly porous, permeable rocks. Overall, these findings indicate that the influence of pore structure on reducing available diffusion area and creating tortuous pathways is more pronounced in low porosity and low-permeability rocks compared to rocks with porosity and permeability higher than approximately 15% and $0.1{\cdot}10^{-12}$ m^2, respectively. Furthermore, the inverse relationship between effective diffusivity and tortuosity, illustrated in Fig. 7d, confirms that gas molecules move more freely through a porous medium with lower tortuosity (Li et al. 2016, 2006; Lou et al. 2021; Lv et al. 2019). Similar observations were reported by Gao et al. (2019) regarding the diffusivity of CO_2 within oil-saturated porous media, with permeabilities ranging from $1.97{\cdot}10^{-14}$ to $2.24{\cdot}10^{-12}$ m^2. Their findings showed a significant initial increase in diffusivity, followed by stabilization for permeabilities greater than $9.87{\cdot}10^{-14}$ m^2. Additionally, consistent correlations with porosity, permeability, and tortuosity have been observed in similar studies exploring CO_2, CH_4, or He diffusion coefficients in water- or oil-saturated rocks of lithologies (Li et al. 2016; Lou et al. 2021; Lv et al. 2019; Pandey et al. 1974). However, some experimental studies have reported a lack of correlation between their observed diffusivities and either porosity or permeability (Li et al. 2006).

While the observed effective gas diffusivities in water-saturated rocks correlate with porosity, permeability, and mean pore size, these relationships have been established using a limited dataset. Hence, it is imperative to conduct further research on various rock types with a wide range of porosity, permeability, and pore size to enhance the reliability of these correlations. Otherwise, individual assessments of any potential reservoir

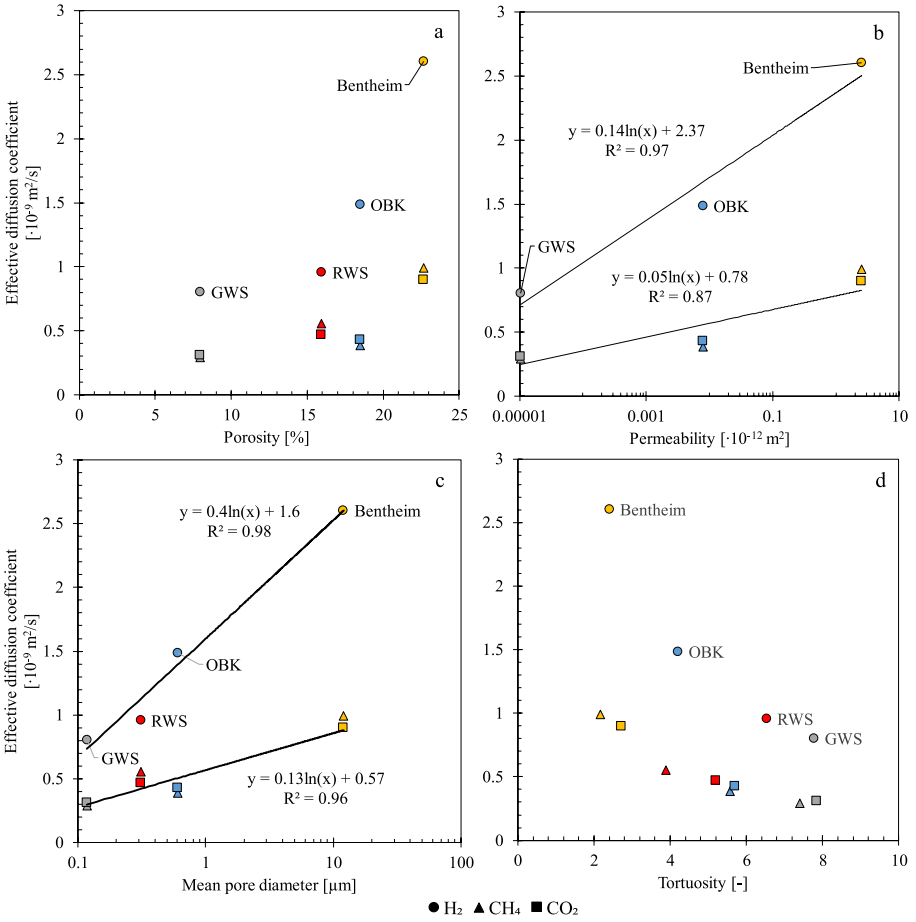

Fig. 7 Correlation of measured effective diffusion coefficients for H_2, CH_4, and CO_2 in the examined rock specimens (fully water-saturated) with **a** porosity, **b** permeability (Arekhov et al. 2023; Nolte et al. 2021; Peksa et al. 2015), **c** mean pore size (Khajooie et al. 2024a), and **d** diffusive tortuosity

involving gas diffusion are necessary to attain a comprehensive understanding of its unique characteristics.

Potential errors in measuring effective diffusivity can likely be attributed to deviations from the assumptions used in developing the mathematical model. Both gas solubility and the gas compressibility factor are pressure-dependent, causing variations in gas concentration at the outer surface of the rock specimen and in the diffusion coefficients, which were assumed to be constant. The pressure drops for H_2 and CH_4 diffusivity tests were negligible (< 0.2%), whereas the CO_2 experiment experienced a 3.5% pressure drop, leading to a proportional reduction in gas concentration. Meanwhile, although the gas compressibility factors increased as the pressure decreased, these changes were considered negligible (even for CO_2). Assuming a direct relationship between gas concentration and effective diffusivity (Li et al. 2006), this suggests that the maximum error due to pressure reduction would be 3.5%. The greater pressure drop observed in CO_2 experiments is primarily due to its higher solubility in water compared to H_2 and CH_4 (Sander 2015). Furthermore, gas

adsorption resulting from gas–rock interactions may occur for all tested gases, albeit to varying extents (Al-Yaseri and Fatah 2024; Ding et al. 2022). However, given the low clay content of the rock specimens (Khajooie et al. 2024b) and their fully water-saturated condition (Grekov et al. 2023), this effect is anticipated to be minimal.

4.6 Implications of Diffusion Coefficient to Underground Hydrogen Storage

This investigation demonstrated that the pressure decay technique is effective in assessing the diffusivity of various gases, from relatively low to highly soluble, in both water and water-saturated rocks. The analyzed rock specimens, collected from four sandstone formations, serve as analogues for hydrogen reservoirs with varying permeability, exhibiting porosities from 8 to 24%. While the effective diffusion coefficients measured offer significant insights, they may not fully represent subsurface conditions due to the absence of in situ stresses and potential alterations from weathering processes as the rock specimens were retrieved from surface mines. Differences between the saturating fluid used in the experiments and in situ formation fluids may also affect the transport characteristics. Nonetheless, the effective diffusivities obtained here provide valuable information for estimating potential gas loss during underground storage and enhance our understanding of the impact of gas diffusion on abiotic and biotic reactions.

The loss of hydrogen is directly related to the square root of the effective diffusion coefficient (Ghaedi et al. 2023). In addition, the relatively smaller molecular size and higher diffusivity of H_2 compared to other gases, such as CH_4 and CO_2, under similar thermophysical conditions, enhance its ability to diffuse through water-saturated rocks (Perera 2023; Zivar et al. 2021). However, a modeling study investigating hydrogen storage in a dormant aquifer with a porosity of 20% and 7 m height within Australia's Cooper Basin indicated a 1% loss from the reservoir during 15 years (Carden and Paterson 1979). The diffusion-driven mass transfer enhances hydrogen saturation within the pore fluid, resulting in a decreased concentration gradient and gradually mitigating diffusive losses over time. Therefore, this effect is particularly significant in the early life of the reservoir or during the initial cycles of cyclic storage (Carden and Paterson 1979; Hassannayebi 2019). Furthermore, in an underground He storage project, it was found that the diffusive loss remained negligible, despite He exhibiting a higher diffusivity compared to H_2 (Hart 1997).

During UHS or biological methanation, the occurrence of microbial metabolism depends on the availability of H_2 molecules as electron donors in the aqueous phase. Thus, the process of mass transfer from the gas to the liquid phase constrains the substrate supply, thereby influencing microbial reactions and, subsequently, the rate of H_2 conversion (Dupnock and Deshusses 2019). Gas transport into the liquid phase is governed by the principles of the two-film theory, a conceptual framework describing this physical processes (Lewis and Whitman 1924). According to this model, the rate of gas–liquid mass transfer depends on the concentration gradient, the mass transfer coefficient, and the gas–liquid interfacial area. The mass transfer coefficient represents the cumulative resistance for transporting gas molecules through the gas and liquid film layers surrounding the gas–liquid interface. Nonetheless, studies have shown that diffusional resistance within the stagnant gas film is negligible, with the mass transfer coefficient primarily controlled by the liquid side (Jensen et al. 2021). This parameter, in turn, is closely linked to both the gas diffusion coefficients in the liquid and the film thickness (Charpentier 1981; Villadsen et al. 2011). Therefore, measuring effective gas diffusivities provides valuable insight into understanding and quantifying gas supply required for

microbial metabolisms. However, microbial activity influences the concentration gradient, another parameter controlling the transfer process. The conversion of hydrogen by microorganisms results in higher or at least sustained concentration gradients compared to those observed in the pure diffusion process (Jensen et al. 2021). This highlights a consistent and indirect effect of H_2 diffusivity on the rate of biological hydrogen conversion. The loss of hydrogen due to biological processes significantly contributes to the total loss during storage in subsurface formations (Liu et al. 2023; Perera 2023). This emphasizes the subtle yet critical importance of accurately determining H_2 diffusivity. It is worth mentioning that the selection of gases for experiments conducted on water-saturated rock specimens in this study was tailored to those implicated in methanogenic reactions during underground hydrogen storage or biological methanation.

5 Conclusions and Outlook

This research systematically investigated the diffusion coefficients of various gases in both water and water-saturated rocks using the pressure decay technique. The measured diffusivities in water for H_2, CH_4, and He at pressures above ambient conditions (0.2 to 1.0 MPa) were consistent with literature values obtained through direct methods, where diffusion coefficients are determined through gas concentration analysis. Additionally, the employed method demonstrated good reproducibility, delivering consistent results across different cells and thereby confirming its reliability for diffusivity assessments. However, the discrepancy observed between the diffusion coefficients of CO_2 and Ar in water and those reported in the literature is likely due to the effect of density-driven convection. This phenomenon occurs as CO_2 and Ar gas molecules dissolve, forming a denser layer at the gas–liquid interface due to their higher density in the aqueous phase relative to water.

The effective diffusivities showed positive correlations with porosity, permeability, and pore diameter, supporting the increased effective area for diffusion and the reduced tortuosity of transport pathways as these parameters increase. This relationship is further evidenced by the inverse correlation between effective diffusion coefficients and tortuosity. The CO_2 diffusion coefficient in water can be calculated using the effective diffusivities measured in the analyzed rock samples, together with tortuosity values derived from H_2 or CH_4 measurements. The results agree with published data, indicating that the presence of porous media or the horizontal diffusive flow direction impedes density-driven convection.

The diffusion process plays a significant role in supporting substrate supply for biotic reactions during UHS. Therefore, integrating diffusion models with kinetic microbial growth models can provide a comprehensive understanding of the interplay between diffusion and biotic processes. Furthermore, there is a scarcity of experimental data on H_2 diffusivity across various rock types, such as sandstone, mudstone, and claystone, under different conditions of pressure, temperature, water salinity, and presence of hydrocarbon. The methodology and experimental setup employed in this study provide a straightforward and reliable approach for future studies intended to bridge this knowledge gap in data within this area of research. Further research on H_2 diffusivity in claystone and mudstone could provide critical insights into the H_2 loss through caprocks (Michelsen et al. 2023; Salina Borello et al. 2024). Additionally, these measurements are essential for estimating the H_2 diffusive flux from potential host formations intended for radioactive waste storage (Bardelli et al. 2014; Jacops et al. 2015; Rebour et al. 1997).

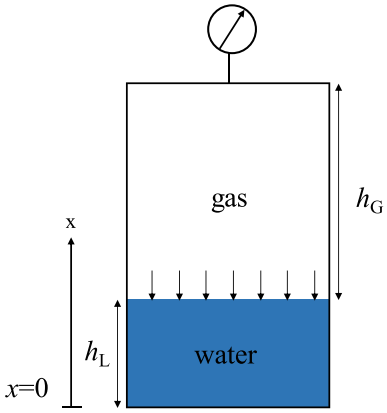

Fig. 8 Physical model of gas diffusion in water during a pressure decay experiment. h_G and h_L denote the heights of gas and water in the diffusion cell, respectively (after Ratnakar and Dindoruk (2015))

Appendix A

Mathematical Model to Determine the Diffusion Coefficient in Water

Ratnakar and Dindoruk (2015) proposed a mathematical model for the pressure decay test aimed at determining the gas diffusion coefficient in liquids using a 1D transient-diffusion model. The study aligns with previous research on gas diffusion in liquids, making similar assumptions in deriving the analytical solution to the diffusion problem (Reza Etminan et al. 2013; Sheikha et al. 2005). These include a constant diffusion coefficient, isothermal conditions, negligible swelling of the liquid, negligible spatial concentration gradient in the gas phase, and no natural or induced convection.

As illustrated in Fig. 8, the gas dissolves in water at the gas/water interface from the top, generating a concentration gradient along a singular direction (the x-axis). Therefore, the gas diffusion process can be described by Fick's second law of diffusion, which states (Crank 1979; Fick 1855; Ratnakar and Dindoruk 2015):

$$\frac{\partial C(x,t)}{\partial t} = D\frac{\partial^2 C(x,t)}{\partial x^2} \tag{A1}$$

where $C(x,t)$ is the concentration of gas in the liquid phase [mol/m^3], and D is the gas diffusion coefficient [m^2/s]. The initial and boundary conditions considered for the diffusion problem are as follows:

$$C(x,0) = 0 \tag{A2a}$$

$$V_g\frac{\partial \rho_g}{\partial t} = AD\frac{\partial C(h_L,t)}{\partial x} \tag{A2b}$$

$$\frac{\partial C(0,t)}{\partial x} = 0 \tag{A2c}$$

At the beginning of the experiment, the gas concentration in water is considered zero (Eq. A2a). The interface boundary condition (at $= h_L$) is defined based on mass conservation within the diffusion cell, where the rate of gas leaving the gas phase equals the

rate of gas diffusion into the liquid. In Eq. A2b, V_g represents the gas phase volume, A the cross-sectional area of the gas–liquid interface, $\rho_g(t)$ the gas molar density at any given time [mol/m^3] and h_L the height of water in the diffusion cell [m] (Fig. 8). Gas density is dependent on gas pressure and can be determined by the real gas law, which is expressed as follows:

$$\rho_g(P,T) = \frac{\mathrm{PMw}}{\mathrm{ZR}(T+273.15)} \tag{A3}$$

where P refers to the gas pressure [Pa], Mw the molecular weight [kg/kmol], Z the gas compressibility factor [−], R the universal gas constant, [8.314·10^3 J/(kmol·K)], and T the temperature [℃]. The second boundary condition assumes a no-flow boundary at the bottom of the cell (Eq. A2c). The gas concentration in water at the gas/water interface (C_{in}) is determined by the solubility of the specific gas in water which is related to gas density ($\rho_g \propto P$) with the proportionality of Henry's constant (H_{cc}) at constant temperature:

$$C\left(h_L,t\right) = C_{in}(t) = \mathrm{H_{cc}}\rho_g(t) \tag{A4}$$

Thus, the inner boundary condition can be formulated as a function of gas concentration in the liquid by combining Eqs. A4 and A2b:

$$\frac{V_g}{\mathrm{H_{cc}}}\frac{\partial \mathrm{C}}{\partial \mathrm{t}} = \mathrm{AD}\frac{\partial \mathrm{C}(h_L,t)}{\partial \mathrm{x}} \tag{A5}$$

The exact solution to Eq. A1, considering the initial and boundary conditions, was derived using the Laplace transform method and can be simplified for relatively long experimental times as follows:

$$\rho_g(t) - \rho_{g\infty} = \beta\exp(\gamma t), \beta = \frac{2\rho_{g0}}{\left(1+\alpha H_{cc}+\frac{\lambda_1^2}{\alpha H_{cc}}\right)}, \text{ and } \gamma = \frac{-\lambda_1^2 D}{h_L^2} \tag{A6}$$

Here, subscripts ∞ and 0 denote the equilibrium and initial conditions for gas density [kg/m^3], respectively, β is the rate coefficient of pressure decay representing the driving force behind the dissolution process [kg/m^3], γ refers to the exponent factor indicating the rate of pressure decay at late times [1/s], α is the volume ratio of the liquid phase to gas phase, and λ_1 is the first root of the following equation:

$$\tan\left(\lambda_i\right) = -\frac{\lambda_i}{\alpha H_{cc}} \tag{A7}$$

In cases where the values of αH_{cc} are small, an approximation for λ_1 can be expressed as:

$$\lambda_1 \to \frac{\pi}{2} + \frac{2}{\pi}\alpha H_{cc} \text{ with } \alpha H_{cc} \ll 1 \tag{A8}$$

The late-transient solution (Eq. A6) is only valid after transition time ($t_{tr} \geq \frac{1}{3\gamma}$). With the average diffusion coefficient of the gases studied in this research ($\approx$4.4·10^{-9} m^2/s) and h_L of 0.03 m, the initial estimate for the transition time is approximately 7.6 h, assuming that $\alpha H_{cc} \to 0$.

Prior to application of this model to the experimental data, the volumes of liquid (V_L) and gas (V_g) phases [cm^3] need to be determined as follows:

$$V_g = \frac{(P_{\mathrm{rc}} - P_{\mathrm{eq}})}{(P_{\mathrm{eq}} - P_{\mathrm{ini}})} V_{\mathrm{rc}}$$

$$V_L = V_{\mathrm{dc}} - V_g \tag{A9}$$

where P_{rc} and P_{ini} are the pressures in the reference and diffusion cells before gas expansion, respectively [Pa], P_{eq} is the initial pressure in the diffusion cell after gas expansion [Pa], and V_{rc} and V_{dc} represent the calibrated volumes of the reference and diffusion cells, respectively [m^3]. The parameter α can then be easily calculated by dividing V_L by V_g. Additionally, the heights of the gas (h_g) and liquid (h_L) columns [m] can be determined by dividing V_g and V_L by the cross- sectional area of the diffusion cell, which is calculated based on the measured cell geometry.

If the pressure decay experiment is conducted until equilibrium, the $\rho_{g\infty}$ can be determined using the pressure value at equilibrium. Nevertheless, it is feasible to assess the experimental data prior to reaching equilibrium, using the following equation to determine $\rho_{g\infty}$:

$$\rho_{g\infty} = \frac{\rho_{g0}}{1 + \alpha H_{\mathrm{cc}}} \tag{A10}$$

where Henry's constant can be obtained from published literature (Sander 2015). Next, the evaluation of experimental data involves plotting $\ln\left(\rho_g(t) - \rho_{g\infty}\right)$ against time, resulting in a linear relationship with a slope of γ and an intercept of $\ln(\beta)$, especially evident after the transition time. Subsequently, the experimental density data can be fitted to the model (Eq. A6) using an optimization algorithm. This process employs the estimated $\rho_{g\infty}$, β, and γ as initial values to accurately determine their values and adjust the transition time accordingly. Once these three variables are determined, the diffusivity can be estimated using Eq. A6, given that the values of λ_1 and h_L are already known. Ratnakar and Dindoruk (2015) provide a comprehensive derivation of this mathematical model and the evaluation procedures.

Mathematical Model to Determine the Effective Diffusion Coefficient in Water-Saturated Rock

Li et al. (2006) introduced a physical model (Fig. 9) elucidating the radial diffusion of gas through water-saturated rocks, subsequently formulating a mathematical model to determine the gas diffusivity. As illustrated in Fig. 9, gas penetration into the water-saturated rock is constrained to occur solely along the radial direction, achieved by sealing the two end faces of the rock specimen.

To develop a mathematical model for gas diffusion in a water-saturated rock specimen, certain simplifying assumptions were established (Li et al. 2006). It was assumed that the gas concentration within the water on the surface of the rock specimen remained constant throughout the experimental duration. The degree of pressure loss was recognized to be influenced by both gas solubility and the volume of water occupying the pore space. Notably, the volume of water within the rock specimen's pores was found to be significantly lower, by one or two orders of magnitude, than the standard volumes typically employed in gas diffusivity

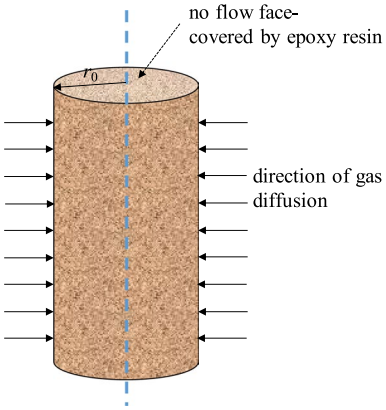

Fig. 9 Physical model of gas diffusion into water-saturated rock specimens along radial direction during a pressure decay test. The two end faces of the rock specimen were sealed with epoxy resin (after Li et al. (2006)). r_0 denotes the radius of the rock plug

assessments (10–20 mL). Consequently, variations in gas concentration at the gas/water interface during diffusivity tests on water were deemed essential to consider, whereas alterations in this parameter at the rock specimen's surface could be safely disregarded. Additionally, it was presumed that the effective diffusion coefficient of gas within the water-saturated rock specimen remained constant under dilute conditions. The rock was also assumed to exhibit homogeneity and isotropy, resulting in a uniform distribution of water throughout the sample. Furthermore, the potential effects arising from natural convection due to density differences in the liquid phase, liquid phase swelling resulting from gas dissolution, and water evaporation into the gas phase were considered negligible. Then, the rate of gas diffusion into water-saturated porous media was determined to be proportional to its concentration gradient, as derived from the integration of Fick's law and the continuity equation (Crank 1979; Li et al. 2006):

$$\frac{\partial \mathrm{C}(t)}{\partial \mathrm{t}} = \frac{D_{\mathrm{eff}}}{r}\frac{\partial}{\partial r}\left(r\frac{\partial C}{\partial r}\right) \tag{A11}$$

where C denotes the gas concentration in the water-saturated porous medium [mol/m^3]; D_{eff} is the effective diffusion coefficient [m^2/s]; t the time [s]; and r is the radius of rock specimen [m]. The initial and boundary conditions for this physical model are as follows:

$$C = C_0 \text{ and } r(t) = r_0 \text{ with } t \geq 0 \tag{A12a}$$

$$C = 0 \text{ and } 0 < r < r_0 \text{ with } t = 0 \tag{A12b}$$

where C_0 denotes the gas concentration in the water at the surface of rock specimen, and r_0 the radius of rock specimen [m]. According to Henry's law, C_0 is directly proportional to the gas pressure at a constant temperature, as stated below:

$$P = H_{\mathrm{cc}} C_0 \tag{A13}$$

Then the solution to Eq. A11 is as follows:

$$\frac{C}{C_\infty} = 1 - \frac{2}{r_0}\sum_{n=1}^{\infty}\frac{\exp(-D_{\mathrm{eff}}\alpha_n^2 \mathrm{t})J_0(r\alpha_n)}{\alpha_n J_1(r\alpha_n)} \tag{A14}$$

where $J_0(x)$ and $J_1(x)$ represent the first kind of Bessel function of zero and first order, respectively, and α_n are the positive roots of the following function:

$$J_0\left(r\alpha_n\right) = 0 \tag{A15}$$

The quantity of gas that has diffused into the water-saturated porous medium can be derived from Eq. A14 and is expressed as (Crank 1979; Li et al. 2006):

$$\frac{N}{N_\infty} = 1 - \sum_{n=1}^{\infty} \frac{4}{r_0^2 \alpha_n^2} \exp(-D_{\text{eff}} \alpha_n^2 \text{t}) \tag{A16}$$

where N refers to the amount of gas diffused in water [mol] at time t, N_∞ is the maximum amount of gas that will eventually diffuse into water [mol].

The maximum gas concentration in water arises from gas dissolution at the surface of the rock specimen. Therefore, N_∞ can be determined by multiplying C_0 and the water volume within the porous media. According to the mass balance, the observed pressure reduction during the experiment can be attributed to the diffusion of gas molecules into the liquid phase. The relationship between pressure and the quantity of gas loss is defined by the real gas law:

$$N = \Delta n = \frac{\Delta P_{\text{g}} V_{\text{g}}}{ZRT} \tag{A17}$$

where Δn represents the amount of gas lost [mol], ΔP_{g} refers to the pressure drop [Pa], V_{g} denotes the gas phase volume (i.e., the sum of the reference cell and the diffusion volumes, excluding the bulk volume of the rock specimen) [m^3], Z is the gas compressibility, R is the universal gas constant [8.314 J/(mol·K)], and T is temperature [K].

Combining Eqs. A17 and A16 yields

$$\Delta P_g = \frac{ZRTN_\infty}{V_g}\left(1 - \sum_{n=1}^{\infty} \frac{4}{r_0^2 \alpha_n^2} \exp\left(-D_{eff} \alpha_n^2 t\right)\right) \tag{A18}$$

In this equation, the only variable that remains unknown is D_{eff}, which can be estimated by fitting the experimental ΔP_{g} with the model outlined in Eq. A18 (Li et al. 2006).

In addition, Li et al. (2006) have shown that for $\sqrt{\frac{\text{D}_{\text{eff}}\text{t}}{\text{r}_0^2}} < 0.1$, Eq. A18 can be approximated with high accuracy with the following relation:

$$\frac{N}{N_\infty} \approx 4\sqrt{\frac{D_{\text{eff}} t}{\pi r_0^2}} \tag{A19}$$

Substituting this term into Eq. A17 yields

$$\Delta P_g = k_1 \sqrt{t} \tag{A20}$$

with

$$k_1 = \frac{4\text{ZRTN}_\infty}{r_0 \text{V}_\text{g}} \sqrt{\frac{D_{\text{eff}}}{\pi}} \tag{A21}$$

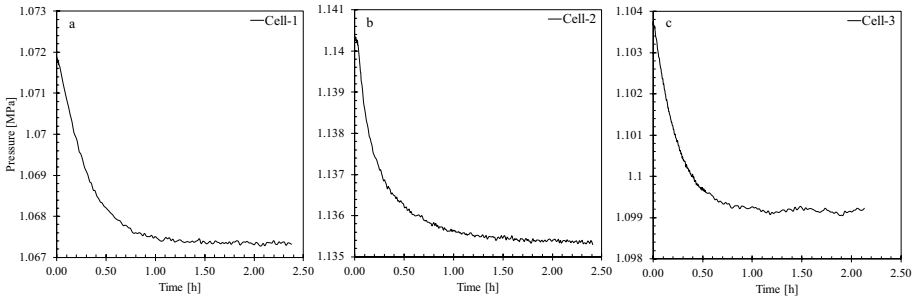

Fig. 10 Pressure decays observed during the so-called blank experiments to investigate the pressure transducers reading in **a** cell-1, **b** cell-2 **b**, and **c** cell-3. It was observed that substantial portion of pressure decay in each cell occurred within less than one hour

Equation A20 clearly demonstrates a linear relationship between the ΔP_g and $\sqrt{t}$, with the slope k_1. Thus, D_{eff} can be obtained from Eq. A21, based on the slope derived from the measured ΔP_g versus $\sqrt{t}$. This resultant value then serves as an initial estimate in Eq. A18, ultimately leading to a precise determination of D_{eff}.

Blank Experiments

To investigate the baseline behavior of pressure transducers, a series of control experiments, referred to as blank experiments, were conducted using empty diffusion cells prior to initiating tests on water and water-saturated rock specimens. In these experiments, helium was injected into cells 1, 2, and 3 at a pressure of approximately 1.0 MPa, consistent with the pressure used in diffusion experiments. Observations revealed pressure drops of 0.0048, 0.0053, and 0.0047 MPa in cells 1, 2, and 3, respectively, with the majority of the decline occurring within the first 30 min (Fig. 10a–c). The reasons for this phenomenon remain unknown to the authors, but it is likely related to the Joule–Thomson effect, deficiencies of pressure transducers, gas diffusion into the membrane, or the capillary restrictions.

Author Contributions Saeed Khajooie contributed to methodology, validation, formal analysis, investigation, data curation, writing—original draft, and visualization. Garri Gaus contributed to conceptualization, writing—review and editing, project administration, and funding acquisition. Timo Seemann performed writing—review and editing. Benedikt Ahrens performed review and editing. Tian Hua contributed to review and editing, and funding acquisition. Ralf Littke performed review and editing, and supervision.

Funding Open Access funding enabled and organized by Projekt DEAL. This study was conducted under the H2_ReacT (FKZ 03G0870C) and H2_ReacT2 (FKZ 03G0902C) projects, funded by the Federal Ministry of Education and Research (BMBF, Germany). It involved collaboration between RWTH Aachen University, BGR, and GFZ, as a component of the GEO: N program on "Utilization of Subsurface Geosystems". In addition, this work was supported by the National Natural Science Foundation of China (Grant 42002177) and the PetroChina R&D Program (Grant YGJ2019-05).

Data Availability The datasets generated during and/or analyzed during the current study are available from the corresponding author on reasonable request.

Declarations

Conflict of interest The authors have no relevant financial or non-financial interests to disclose.

References

Aftab, A., Hassanpouryouzband, A., Martin, A., Kendrick, J.E., Thaysen, E.M., Heinemann, N., Utley, J., Wilkinson, M., Haszeldine, R.S., Edlmann, K.: Geochemical integrity of wellbore cements during geological hydrogen storage. Environ. Sci. Technol. Lett. **10**(7), 551–556 (2023). https://doi.org/10.1021/acs.estlett.3c00303

Aikazyan, E.A., Fedorova, I.A.: Determination of the diffusion coefficient of H2 by electrochemical method. Dokl. Akad. Nauk (Russian) **86**, 1137–1140 (1952)

Al-Yaseri, A., Fatah, A.: Impact of H2-CH4 mixture on pore structure of sandstone and limestone formations relevant to subsurface hydrogen storage. Fuel **358**, 130192 (2024). https://doi.org/10.1016/j.fuel.2023.130192

Amann-Hildenbrand, A., Krooss, B.M., Harrington, J., Cuss, R., Davy, C., Skoczylas, F., Jacops, E., Maes, N.: Chapter 7 - gas transfer through clay barriers. In: Tournassat, C., Steefel, C.I., Bourg, I.C., Bergaya, F. (eds.) Developments in clay science, vol. 6, pp. 227–267. Elsevier, Amsterdam (2015). https://doi.org/10.1016/B978-0-08-100027-4.00007-3

Arekhov, V., Zhainakov, T., Clemens, T., Wegner, J.: Measurement of effective hydrogen-methane gas diffusion coefficients in reservoir rocks. SPE Reserv. Eval. Eng. **26**(04), 1242–1257 (2023). https://doi.org/10.2118/214451-PA

Baird, M.H.I., Davidson, J.F.: Annular jets—II: gas absorption. Chem. Eng. Sci. **17**(6), 473–480 (1962). https://doi.org/10.1016/0009-2509(62)85016-7

Bardelli, F., Mondelli, C., Didier, M., Vitillo, J.G., Cavicchia, D.R., Robinet, J.-C., Leone, L., Charlet, L.: Hydrogen uptake and diffusion in Callovo-Oxfordian clay rock for nuclear waste disposal technology. Appl. Geochem. **49**, 168–177 (2014). https://doi.org/10.1016/j.apgeochem.2014.06.019

Bear, J.: Dynamics of fluids in porous media. Elsevier, New York (1972)

Bennett, L., Ng, W.Y., Walkley, J.: Diffusion of gases in nonpolar liquids. Open-tube method. J. Phys. Chem. **72**(13), 4699–4700 (1968)

Berta, M., Dethlefsen, F., Ebert, M., Schafer, D., Dahmke, A.: Geochemical effects of millimolar hydrogen concentrations in groundwater: an experimental study in the context of subsurface hydrogen storage. Environ. Sci. Technol. **52**(8), 4937–4949 (2018). https://doi.org/10.1021/acs.est.7b05467

Blair, L.M., Quinn, J.A.: The onset of cellular convection in a fluid layer with time-dependent density gradients. J. Fluid Mech. **36**(2), 385–400 (1969). https://doi.org/10.1017/S0022112069001716

Cadogan, S.P., Maitland, G.C., Trusler, J.P.M.: Diffusion coefficients of CO_2 and N_2 in water at temperatures between 29815 K and 42315 K at pressures up to 45 MPa. J. Chem. Eng. Data **59**(2), 519–525 (2014). https://doi.org/10.1021/je401008s

Carden, P.O., Paterson, L.: Physical, chemical and energy aspects of underground hydrogen storage. Int. J. Hydrogen Energy **4**(6), 559–569 (1979). https://doi.org/10.1016/0360-3199(79)90083-1

Caskey, J.A., Michelsen, D.L., To, Y.P.: The effect of surfactant hydrophilic group on gas absorption rates. J. Colloid Interface Sci. **42**(1), 62–69 (1973). https://doi.org/10.1016/0021-9797(73)90007-6

Charlet, L., Alt-Epping, P., Wersin, P., Gilbert, B.: Diffusive transport and reaction in clay rocks: a storage (nuclear waste, CO_2, H_2), energy (shale gas) and water quality issue. Adv. Water Resour. **106**, 39–59 (2017). https://doi.org/10.1016/j.advwatres.2017.03.019

Charpentier, J.-C.: Mass-transfer rates in gas-liquid absorbers and reactors. In: Drew, T.B., Cokelet, G.R., Hoopes, J.W., Vermeulen, T. (eds.) Advances in chemical engineering, vol. 11, pp. 1–133. Academic Press, New York (1981). https://doi.org/10.1016/S0065-2377(08)60025-3

Chen, Y.A., Chu, C.K., Chen, Y.P., Chu, L.S., Lin, S.T., Chen, L.-J.: Measurements of diffusion coefficient of methane in water/brine under high pressure. Terr. Atmos. Ocean. Sci. J. (2018). https://doi.org/10.3319/TAO.2018.02.23.02

Chilingar, G.V.: Relationship between porosity, permeability, and grain-size distribution of sands and sandstones. In: van Straaten, L.M.J.U. (ed.) Developments in sedimentology, vol. 1, pp. 71–75. Elsevier, Amsterdam (1964). https://doi.org/10.1016/S0070-4571(08)70469-2

Crank, J.: The mathematics of diffusion. Oxford University Press, Oxford (1979)

Cussler, E.L.: Diffusion: mass transfer in fluid systems. Cambridge University Press, Cambridge (1997)

da Silva, M.T., do Rocio Cardoso, M., Veronese, C.M., Mazer, W.: Tortuosity: a brief review. Mater. Today Proc. **1**(58), 1344–9 (2022)

Dabbaghi, E., Ng, K., Brown, T.C., Yu, Y.: Experimental study on the effect of hydrogen on the mechanical properties of hulett sandstone. Int. J. Hydrogen Energy **60**, 468–478 (2024). https://doi.org/10.1016/j.ijhydene.2024.02.210

Das, S.K., Butler, R.M.: Diffusion coefficients of propane and butane in peace river bitumen. Can. J. Chem. Eng. **74**(6), 985–992 (1996). https://doi.org/10.1002/cjce.5450740623

Davidson, J.F.: The determination of diffusion coefficient for sparingly soluble gases in liquids. Trans. Inst. Chem. Engrs. **35**, 51–60 (1957)

Ding, J., Yan, C., Wang, G., He, Y., Zhao, R.: Competitive adsorption between CO_2 and CH_4 in tight sandstone and its influence on CO_2-injection enhanced gas recovery (EGR). Int. J. Greenhouse Gas Control **113**, 103530 (2022). https://doi.org/10.1016/j.ijggc.2021.103530

Dopffel, N., Jansen, S., Gerritse, J.: Microbial side effects of underground hydrogen storage—knowledge gaps, risks and opportunities for successful implementation. Int. J. Hydrogen Energy **46**(12), 8594–8606 (2021). https://doi.org/10.1016/j.ijhydene.2020.12.058

Duan, Z., Mao, S.: A thermodynamic model for calculating methane solubility, density and gas phase composition of methane-bearing aqueous fluids from 273 to 523 K and from 1 to 2000 bar. Geochim. Cosmochim. Acta **70**(13), 3369–3386 (2006). https://doi.org/10.1016/j.gca.2006.03.018

Dupnock, T.L., Deshusses, M.A.: Detailed investigations of dissolved hydrogen and hydrogen mass transfer in a biotrickling filter for upgrading biogas. Biores. Technol. **290**, 121780 (2019). https://doi.org/10.1016/j.biortech.2019.121780

Ferrell, R.T., Himmelblau, D.M.: Diffusion coefficients of hydrogen and helium in water. AIChE J. **13**(4), 702–708 (1967). https://doi.org/10.1002/aic.690130421

Fick, A.: Ueber diffusion. Ann. Phys. **170**(1), 59–86 (1855). https://doi.org/10.1002/andp.18551700105

Fleury, M., Berne, P., Bachaud, P.: Diffusion of dissolved CO_2 in caprock. Energy Proc. **1**(1), 3461–3468 (2009). https://doi.org/10.1016/j.egypro.2009.02.137

Frank, M.J.W., Kuipers, J.A.M., van Swaaij, W.P.M.: Diffusion coefficients and viscosities of $CO_2 + H_2O$, $CO_2 + CH_3OH$, $NH_3 + H_2O$, and $NH_3 + CH_3OH$ liquid mixtures. J. Chem. Eng. Data **41**(2), 297–302 (1996). https://doi.org/10.1021/je950157k

Gao, H., Zhang, B., Fan, L., Zhang, H., Chen, G., Tontiwachwuthikul, P., Liang, Z.: Study on diffusivity of CO_2 in oil-saturated porous media under high pressure and temperature. Energy Fuels **33**(11), 11364–11372 (2019). https://doi.org/10.1021/acs.energyfuels.9b01947

Gaus, G., Amann-Hildenbrand, A., Krooss, B.M., Fink, R.: Gas permeability tests on core plugs from unconventional reservoir rocks under controlled stress: a comparison of different transient methods. J. Nat. Gas Sci. Eng. **65**, 224–236 (2019). https://doi.org/10.1016/j.jngse.2019.03.003

Gertz, K.H., Loeschcke, H.H.: Bestimmung der diffusions-Koeffizienten von H_2, O_2, N_2, und He in Wasser und Blutserum bei konstant gehaltener Konvektion. Z. Naturforschung B **9**(1), 1–9 (1954)

Ghaedi, M., Andersen, P.Ø., Gholami, R.: Hydrogen diffusion into caprock: a semi-analytical solution and a hydrogen loss criterion. J. Energy Storage **64**, 107134 (2023). https://doi.org/10.1016/j.est.2023.107134

Ghanbarian, B., Hunt, A.G., Ewing, R.P., Sahimi, M.: Tortuosity in porous media: a critical review. Soil Sci. Soc. Am. J. **77**(5), 1461–1477 (2013). https://doi.org/10.2136/sssaj2012.0435

Gherardi, F., Audigane, P., Gaucher, E.C.: Predicting long-term geochemical alteration of wellbore cement in a generic geological CO_2 confinement site: tackling a difficult reactive transport modeling challenge. J. Hydrol. **420–421**, 340–359 (2012). https://doi.org/10.1016/j.jhydrol.2011.12.026

Gholami, Y., Azin, R., Fatehi, R., Osfouri, S., Bahadori, A.: Prediction of carbon dioxide dissolution in bulk water under isothermal pressure decay at different boundary conditions. J. Mol. Liq. **202**, 23–33 (2015). https://doi.org/10.1016/j.molliq.2014.11.031

Gill, W.N., Sankarasubramanian, R., Taylor, G.I.: Exact analysis of unsteady convective diffusion. Proc. R. Soc. Lond. Math. Phys. Sci. **316**(1526), 341–350 (1997). https://doi.org/10.1098/rspa.1970.0083

Gnanasekaran, D., Reddy, B.S.R.: Cost effective poly(urethane-imide)-POSS membranes for environmental and energy-related processes. Clean Technol. Environ. Policy **15**(2), 383–389 (2013). https://doi.org/10.1007/s10098-012-0500-7

Grathwohl, P.: Diffusion in natural porous media: contaminant transport, sorption/desorption and dissolution kinetics, 1st edn. Springer, New York (1998). https://doi.org/10.1007/978-1-4615-5683-1

Grekov, D.I., Robinet, J.-C., Grambow, B.: Adsorption of methane and carbon dioxide by water-saturated clay minerals and clay rocks. Appl. Clay Sci. **232**, 106806 (2023). https://doi.org/10.1016/j.clay.2022.106806

Grogan, A.T., Pinczewski, V.W., Ruskauff, G.J., Orr, F.M., Jr.: Diffusion of CO_2 at reservoir conditions: models and measurements. SPE Reserv. Eng. **3**(01), 93–102 (1988). https://doi.org/10.2118/14897-PA

Gubbins, K.E., Bhatia, K.K., Walker, R.D.: Diffusion of gases in electrolytic solutions. AIChE J. **12**(3), 548–552 (1966). https://doi.org/10.1002/aic.690120328

Guo, H., Chen, Y., Lu, W., Li, L., Wang, M.: In situ Raman spectroscopic study of diffusion coefficients of methane in liquid water under high pressure and wide temperatures. Fluid Phase Equilib. **360**, 274–278 (2013). https://doi.org/10.1016/j.fluid.2013.09.051

Hanebeck, D.: Experimentelle Simulation und Untersuchung der Genese und Expulsion von Erdölen aus Muttergesteinen [E-Book]. Forschungszentrum, Zentralbibliothek. ISBN: http://hdl.handle.net/2128/21296 (1995)

Hanson, A. G., Kutchko, B., Lackey, G., Gulliver, D., Strazisar, B. R., Tinker, K. A., Haeri, F., Wright, R., Huerta, N., Baek, S., Bagwell, C., Toledo Camargo, J. d., Freeman, G., Kuang, W., Torgeson, J., White, J., Buscheck, T., Castelletto, N., Smith, M.: Subsurface hydrogen and natural gas storage: state of knowledge and research recommendations report. https://www.osti.gov/biblio/1846632 (2022)

Harrington, J.F., Milodowski, A.E., Graham, C.C., Rushton, J.C., Cuss, R.J.: Evidence for gas-induced pathways in clay using a nanoparticle injection technique. Mineral. Mag. **76**(8), 3327–3336 (2012). https://doi.org/10.1180/minmag.2012.076.8.45

Hart, D.: Hydrogen power : the commerical future of 'the ultimate fuel'. Financial Times Energy Pub, a division of Pearson Professional Limited. ISBN: 1853347604 https://cir.nii.ac.jp/crid/1130000794060174848 (1997)

Hassannayebi, N.: An assessment of underground hydrogen storage: Transport, geochemistry, and bioactivity. Doctoral Thesis, Montanuniversitaet Leoben. https://pure.unileoben.ac.at/en/publications/an-assessment-of-underground-hydrogen-storage-transport-geochemis (2019)

Hassanpouryouzband, A., Adie, K., Cowen, T., Thaysen, E.M., Heinemann, N., Butler, I.B., Wilkinson, M., Edlmann, K.: Geological hydrogen storage: geochemical reactivity of hydrogen with sandstone reservoirs. ACS Energy Lett. **7**(7), 2203–2210 (2022). https://doi.org/10.1021/acsenergylett.2c01024

Heinemann, N., Alcalde, J., Miocic, J.M., Hangx, S.J.T., Kallmeyer, J., Ostertag-Henning, C., Hassanpouryouzband, A., Thaysen, E.M., Strobel, G.J., Schmidt-Hattenberger, C., Edlmann, K., Wilkinson, M., Bentham, M., Stuart Haszeldine, R., Carbonell, R., Rudloff, A.: Enabling large-scale hydrogen storage in porous media—the scientific challenges. Energy Environ. Sci. **14**(2), 853–864 (2021). https://doi.org/10.1039/d0ee03536j

Hogeweg, S., Michelsen, J., Hagemann, B., Ganzer, L.: Empirical and numerical modelling of gas-gas diffusion for binary hydrogen-methane systems at underground gas storage conditions. Transp. Porous Med. **151**(1), 213–232 (2024). https://doi.org/10.1007/s11242-023-02039-8

Holzer, L., Wiedenmann, D., Münch, B., Keller, L., Prestat, M., Gasser, P., Robertson, I., Grobéty, B.: The influence of constrictivity on the effective transport properties of porous layers in electrolysis and fuel cells. J. Mater. Sci. **48**(7), 2934–2952 (2013). https://doi.org/10.1007/s10853-012-6968-z

Holzer, L., Marmet, P., Fingerle, M., Wiegmann, A., Neumann, M., Schmidt, V.: Tortuosity-porosity relationships: review of empirical data from literature. In: Holzer, L., Marmet, P., Fingerle, M., Wiegmann, A., Neumann, M., Schmidt, V. (eds.) Tortuosity and microstructure effects in porous media: classical theories, empirical data and modern methods, pp. 51–89. Springer International Publishing, Cham (2023)

Houghton, G., Ritchie, P.D., Thomson, J.A.: The rate of solution of small stationary bubbles and the diffusion coefficients of gases in liquids. Chem. Eng. Sci. **17**(4), 221–227 (1962). https://doi.org/10.1016/0009-2509(62)85001-5

Hu, Z., Gaus, G., Seemann, T., Zhang, Q., Littke, R., Fink, R.: Pore structure and sorption capacity investigations of Ediacaran and Lower Silurian gas shales from the Upper Yangtze platform, China. Geomech. Geophys. Geo-Energy Geo-Resour. **7**(3), 71 (2021). https://doi.org/10.1007/s40948-021-00262-5

Hubao, Z.Y., Chen, Y., Ran, H., Wood, C.D., Kang, Q., Chen, Y.F.: H_2 diffusion in cement nanopores and its implication for underground hydrogen storage. J. Energy Storage **102**, 113926 (2024). https://doi.org/10.1016/j.est.2024.113926

Jacops, E., Volckaert, G., Maes, N., Weetjens, E., Govaerts, J.: Determination of gas diffusion coefficients in saturated porous media: He and CH_4 diffusion in Boom Clay. Appl. Clay Sci. **83–84**, 217–223 (2013). https://doi.org/10.1016/j.clay.2013.08.047

Jacops, E., Wouters, K., Volckaert, G., Moors, H., Maes, N., Bruggeman, C., Swennen, R., Littke, R.: Measuring the effective diffusion coefficient of dissolved hydrogen in saturated Boom Clay. Appl. Geochem. **61**, 175–184 (2015). https://doi.org/10.1016/j.apgeochem.2015.05.022

Jacops, E., Aertsens, M., Maes, N., Bruggeman, C., Krooss, B.M., Amann-Hildenbrand, A., Swennen, R., Littke, R.: Interplay of molecular size and pore network geometry on the diffusion of dissolved gases and HTO in Boom Clay. Appl. Geochem. **76**, 182–195 (2017). https://doi.org/10.1016/j.apgeochem.2016.11.022

Jacops, E., Rogiers, B., Frederickx, L., Swennen, R., Littke, R., Krooss, B.M., Amann-Hildenbrand, A., Bruggeman, C.: The relation between petrophysical and transport properties of the Boom Clay and Eigenbilzen Sands. Appl. Geochem. **114**, 104527 (2020). https://doi.org/10.1016/j.apgeochem.2020.104527

Jacops, E.: Development and application of an innovative method for studying the diffusion of dissolved gases in porous saturated media. Doctoral Thesis, RWTH Aachen University. http://publications.rwth-aachen.de/record/748491 (2018)

Jähne, B., Heinz, G., Dietrich, W.: Measurement of the diffusion coefficients of sparingly soluble gases in water. J. Geophys. Res. Oceans **92**(C10), 10767–10776 (1987). https://doi.org/10.1029/JC092iC10p10767

Jamialahmadi, M., Emadi, M., Müller-Steinhagen, H.: Diffusion coefficients of methane in liquid hydrocarbons at high pressure and temperature. J. Petrol. Sci. Eng. **53**(1), 47–60 (2006). https://doi.org/10.1016/j.petrol.2006.01.011

Jensen, M.B., Ottosen, L.D.M., Kofoed, M.V.W.: H2 gas-liquid mass transfer: a key element in biological Power-to-Gas methanation. Renew. Sustain. Energy Rev. **147**, 111209 (2021). https://doi.org/10.1016/j.rser.2021.111209

Jun, Y.-S., Giammar, D.E., Werth, C.J.: Impacts of geochemical reactions on geologic carbon sequestration. Environ. Sci. Technol. **47**(1), 3–8 (2013). https://doi.org/10.1021/es3027133

Khajooie, S., Gaus, G., Seemann, T., Klaver, J., Claes, H., Nehler, M., Ahrens, B., Littke, R.: Methanogenic activity in water-saturated reservoir analogues for underground hydrogen storage: the role of surface area. Int. J. Hydrogen Energy **90**, 171–190 (2024a). https://doi.org/10.1016/j.ijhydene.2024.09.395

Khajooie, S., Gaus, G., Dohrmann, A.B., Krüger, M., Littke, R.: Methanogenic conversion of hydrogen to methane in reservoir rocks: an experimental study of microbial activity in water-filled pore space. Int. J. Hydrogen Energy **50**, 272–290 (2024b). https://doi.org/10.1016/j.ijhydene.2023.07.065

Krooss, B., Schaefer, R.: Experimental measurements of the diffusion parameters of light hydrocarbons in water-saturated sedimentary rocks—I a new experimental procedure. Organ. Geochem. **11**(3), 193–199 (1987). https://doi.org/10.1016/0146-6380(87)90022-2

Krooss, B.M., Leythaeuser, D., Schaefer, R.G.: Light hydrocarbon diffusion in a caprock. Chem. Geol. **71**(1), 65–76 (1988). https://doi.org/10.1016/0009-2541(88)90106-4

Krooss, B.M., Leythaeuser, D., Schaefer, R.G.: The quantification of diffusive hydrocarbon losses through cap rocks of natural gas reservoirs—a reevaluation: reply1. AAPG Bull. **76**(11), 1842–1846 (1992). https://doi.org/10.1306/BDFF8AF6-1718-11D7-8645000102C1865D

Krooss, B.: Evaluation of database on gas migration through clayey host rocks. Report for NIRAS-ONDRAF, RWTH Aachen University.

Kunz, O., Wagner, W.: The GERG-2008 wide-range equation of state for natural gases and other mixtures: an expansion of GERG-2004. J. Chem. Eng. Data **57**(11), 3032–3091 (2012). https://doi.org/10.1021/je300655b

Labus, M., Wertz, F.: Identifying geochemical reactions on wellbore cement/caprock interface under sequestration conditions. Environ. Earth Sci. **76**(12), 443 (2017). https://doi.org/10.1007/s12665-017-6771-x

Lauro, F.M., McDougald, D., Thomas, T., Williams, T.J., Egan, S., Rice, S., DeMaere, M.Z., Ting, L., Ertan, H., Johnson, J., Ferriera, S., Lapidus, A., Anderson, I., Kyrpides, N., Munk, A.C., Detter, C., Han, C.S., Brown, M.V., Robb, F.T., Cavicchioli, R.: The genomic basis of trophic strategy in marine bacteria. Proc. Nat. Acad. Sci. **106**(37), 15527–15533 (2009). https://doi.org/10.1073/pnas.0903507106

Lewis, W.K., Whitman, W.G.: Principles of gas absorption. Ind. Eng. Chem. **16**(12), 1215–1220 (1924). https://doi.org/10.1021/ie50180a002

Li, Z., Dong, M.: Experimental study of diffusive tortuosity of liquid-saturated consolidated porous media. Ind. Eng. Chem. Res. **49**(13), 6231–6237 (2010). https://doi.org/10.1021/ie901765d

Li, Z., Dong, M., Li, S., Dai, L.: A new method for gas effective diffusion coefficient measurement in water-saturated porous rocks under high pressures. J. Porous Med. **9**(5), 445–461 (2006). https://doi.org/10.1615/JPorMedia.v9.i5.50

Li, S., Li, Z., Dong, Q.: Diffusion coefficients of supercritical CO_2 in oil-saturated cores under low permeability reservoir conditions. J. CO_2 Utilization **14**, 47–60 (2016). https://doi.org/10.1016/j.jcou.2016.02.002

Li, Z.: Study of gas diffusion in liquid-saturated porous media for oil recovery and CO_2 sequestration Ph.D. Dissertation, University of Regina, Regina, SK. (2006)

Liu, G., Zhao, Z., Sun, M., Li, J., Hu, G., Wang, X.: New insights into natural gas diffusion coefficient in rocks. Pet. Explor. Dev. **39**(5), 597–604 (2012). https://doi.org/10.1016/S1876-3804(12)60081-0

Liu, N., Kovscek, A.R., Fernø, M.A., Dopffel, N.: Pore-scale study of microbial hydrogen consumption and wettability alteration during underground hydrogen storage. Front. Energy Res. (2023). https://doi.org/10.3389/fenrg.2023.1124621

Lou, X., Chakraborty, N., Karpyn, Z.T., Ayala, L.F., Nagarajan, N., Wijaya, Z.: Experimental study of gas/liquid diffusion in porous rocks and bulk fluids to investigate the effect of rock-matrix hindrance. SPE J. **26**(03), 1174–1188 (2021). https://doi.org/10.2118/195941-PA

Lu, W., Guo, H., Chou, I.M., Burruss, R.C., Li, L.: Determination of diffusion coefficients of carbon dioxide in water between 268 and 473 K in a high-pressure capillary optical cell with in situ Raman spectroscopic measurements. Geochim. Cosmochim. Acta **115**, 183–204 (2013). https://doi.org/10.1016/j.gca.2013.04.010

Lv, J., Chi, Y., Zhao, C., Zhang, Y., Mu, H.: Experimental study of the supercritical CO_2 diffusion coefficient in porous media under reservoir conditions. R. Soc. Open Sci. **6**(6), 181902 (2019). https://doi.org/10.1098/rsos.181902

Maharajh, D.M., Walkley, J.: The temperature dependence of the diffusion coefficients of Ar, CO_2, CH_4, CH_3Cl, CH_3Br, and $CHCl_2F$ in Water. Can. J. Chem. **51**(6), 944–952 (1973). https://doi.org/10.1139/v73-140

Michelsen, J., Hagemann, B., Ganzer, L., & Hujer, W.: Measurement of hydrogen diffusion through caprock samples. In: Sixth International Conference on Fault and Top Seals. pp. 1–5. European Association of Geoscientists & Engineers, Vienna, Austria (2022) https://doi.org/10.3997/2214-4609.202243061

Michelsen, J., Langanke, N., Hagemann, B., Hogeweg, S., Ganzer, L.: Diffusion measurements with hydrogen and methane through reservoir rock samples, In: Advanced SCAL for Carbon Storage & CO_2 Utilization. Presented at the 36th International Symposium of the Society of Core Analysts, Abu Dhabi, UAE, October 12, (2023)

Muller, E., Guélard, J., Sissmann, O., Tafit, A., & Poirier, S.: Evidencing the influence of temperature and mineralogy on microbial competition for hydrogen consumption: Implications for underground hydrogen storage (UHS). International Journal of Hydrogen Energy, 82, 1101–1113 (2024). https://doi.org/10.1016/j.ijhydene.2024.08.024

Nelson, P.H.: Permeability-porosity relationships in sedimentary rocks. Log Anal. **35**(3), 38–62 (1994)

Nolte, S., Fink, R., Krooss, B.M., Littke, R.: Simultaneous determination of the effective stress coefficients for permeability and volumetric strain on a tight sandstone. J. Nat. Gas Sci. Eng. (2021). https://doi.org/10.1016/j.jngse.2021.104186

Oelkers, E.H.: Calculation of diffusion coefficients for aqueous organic species at temperatures from 0 to 350 °C. Geochim. Cosmochim. Acta **55**(12), 3515–3529 (1991). https://doi.org/10.1016/0016-7037(91)90052-7

Ortiz, L., Volckaert, G., Mallants, D.: Gas generation and migration in Boom Clay, a potential host rock formation for nuclear waste storage. Eng. Geol. **64**(2), 287–296 (2002). https://doi.org/10.1016/S0013-7952(01)00107-7

Pandey, G.N., Tek, M.R., Katz, D.L.: Diffusion of fluids through porous media with implications in petroleum geology. AAPG Bull. **58**(2), 291–303 (1974)

Peksa, A.E., Wolf, K.-H.A.A., Zitha, P.L.J.: Bentheimer sandstone revisited for experimental purposes. Mar. Pet. Geol. **67**, 701–719 (2015). https://doi.org/10.1016/j.marpetgeo.2015.06.001

Perera, M.S.A.: A review of underground hydrogen storage in depleted gas reservoirs: insights into various rock-fluid interaction mechanisms and their impact on the process integrity. Fuel **334**, 126677 (2023). https://doi.org/10.1016/j.fuel.2022.126677

Pomeroy, R.D., Lacey, W.N., Scudder, N.F., Stapp, F.P.: Rate of solution of methane in quiescent liquid hydrocarbons. Ind. Eng. Chem. **25**(9), 1014–1019 (1933). https://doi.org/10.1021/ie50285a021

Ratnakar, R.R., Dindoruk, B.: Measurement of gas diffusivity in heavy oils and bitumens by use of pressure-decay test and establishment of minimum time criteria for experiments. SPE J. **20**(05), 1167–1180 (2015). https://doi.org/10.2118/170931-PA

Reamer, H.H., Opfell, J.B., Sage, B.H.: Diffusion coefficients in hydrocarbon systems methane-decane-methane in liquid phase - methane-decane-methane in liquid phase. Ind. Eng. Chem. **48**(2), 275–282 (1956). https://doi.org/10.1021/ie50554a034

Rebour, V., Billiotte, J., Deveughele, M., Jambon, A., le Guen, C.: Molecular diffusion in water-saturated rocks: a new experimental method. J. Contam. Hydrol. **28**(1), 71–93 (1997). https://doi.org/10.1016/S0169-7722(96)00051-4

Reitenbach, V., Ganzer, L., Albrecht, D., Hagemann, B.: Influence of added hydrogen on underground gas storage: a review of key issues. Environmental Earth Sciences **73**(11), 6927–6937 (2015). https://doi.org/10.1007/s12665-015-4176-2

Renkin, E.M.: Filtration, diffusion, and molecular sieving through porous cellulose membranes. J. Gen. Physiol. **38**(2), 225–243 (1954)

Renner, T.A.: Measurement and correlation of diffusion coefficients for CO_2 and rich-gas applications. SPE Reserv. Eng. **3**(02), 517–523 (1988). https://doi.org/10.2118/15391-PA

Reza Etminan, S., Pooladi-Darvish, M., Maini, B.B., Chen, Z.: Modeling the interface resistance in low soluble gaseous solvents-heavy oil systems. Fuel **105**, 672–687 (2013). https://doi.org/10.1016/j.fuel.2012.08.048

Riazi, M.R.: A new method for experimental measurement of diffusion coefficients in reservoir fluids. J. Petrol. Sci. Eng. **14**(3), 235–250 (1996). https://doi.org/10.1016/0920-4105(95)00035-6

Sachs, W.: The diffusional transport of methane in liquid water: method and result of experimental investigation at elevated pressure. J. Petrol. Sci. Eng. **21**(3), 153–164 (1998). https://doi.org/10.1016/S0920-4105(98)00048-5

Sahores, J.J., Witherspoon, P.A.: Diffusion of light paraffin hydrocarbons in water from 2 to 80 °C. In: Hobson, G.D., Speers, G.C. (eds.) Advances in organic geochemistry, pp. 219–230. Pergamon, Oxford (1970). https://doi.org/10.1016/B978-0-08-012758-3.50018-9

Salina Borello, E., Bocchini, S., Chiodoni, A., Coti, C., Fontana, M., Panini, F., Peter, C., Pirri, C.F., Tawil, M., Mantegazzi, A., Marzano, F.: Underground hydrogen storage safety: experimental study of hydrogen diffusion through caprocks. Energies **17**(2), 394 (2024)

Sander, R.: Compilation of Henry's law constants (version 4.0) for water as solvent. Atmos. Chem. Phys. **15**(8), 4399–4981 (2015). https://doi.org/10.5194/acp-15-4399-2015

Schlömer, S., Krooss, B.M.: Experimental characterisation of the hydrocarbon sealing efficiency of cap rocks. Mar. Pet. Geol. **14**(5), 565–580 (1997). https://doi.org/10.1016/S0264-8172(97)00022-6

Schmidt, T.: Mass transfer by diffusion. AOSTRA handbook on oil sands, bitumens and heavy oils; Hepler, L. G., Zhu, X. (Eds). Alberta oil sands technology & research authority (AOSTRA). ISBN: 978-0-7732-0189-7

Sheikha, H., Pooladi-Darvish, M., Mehrotra, A.K.: Development of graphical methods for estimating the diffusivity coefficient of gases in bitumen from pressure-decay data. Energy Fuels **19**(5), 2041–2049 (2005). https://doi.org/10.1021/ef050057c

Shen, L., Chen, Z.: Critical review of the impact of tortuosity on diffusion. Chem. Eng. Sci. **62**(14), 3748–3755 (2007). https://doi.org/10.1016/j.ces.2007.03.041

Song, J., Zhang, D.: Comprehensive review of caprock-sealing mechanisms for geologic carbon sequestration. Environ. Sci. Technol. **47**(1), 9–22 (2013). https://doi.org/10.1021/es301610p

Strauch, B., Pilz, P., Hierold, J., Zimmer, M.: Experimental simulations of hydrogen migration through potential storage rocks. Int. J. Hydrogen Energy **48**(66), 25808–25820 (2023). https://doi.org/10.1016/j.ijhydene.2023.03.115

Tammann, G., Jessen, V.: Über die diffusionskoeffizienten von gasen in wasser und ihre temperaturabhängigkeit. Z. Anorg. Allg. Chem. **179**(1), 125–144 (1929). https://doi.org/10.1002/zaac.19291790110

Tan, K.K., Thorpe, R.B.: Gas diffusion into viscous and non-Newtonian liquids. Chem. Eng. Sci. **47**(13), 3565–3572 (1992). https://doi.org/10.1016/0009-2509(92)85071-I

Tiab, D., Donaldson, E.C.: Chapter 3 - porosity and permeability. In: Tiab, D., Donaldson, E.C. (eds.) Petrophysics, 4th edn., pp. 67–186. Gulf Professional Publishing, Houston (2016). https://doi.org/10.1016/B978-0-12-803188-9.00003-6

Upreti, S.R., Mehrotra, A.K.: Experimental measurement of gas diffusivity in bitumen: results for carbon dioxide. Indus. Eng. Chem. Res. **39**(4), 1080–1087 (2000). https://doi.org/10.1021/ie990635a

Upreti, S.R., Mehrotra, A.K.: Diffusivity of CO_2, CH_4, C_2H_6 and N_2 in Athabasca bitumen. Can. J. Chem. Eng. **80**(1), 116–125 (2002). https://doi.org/10.1002/cjce.5450800112

Villadsen, J., Nielsen, J., Lidén, G.: Bioreaction engineering principles. Springer Science & Business Media, Cham (2011)
Vivian, J.E., King, C.J.: Diffusivities of slightly soluble gases in water. AIChE J. **10**(2), 220–221 (1964). https://doi.org/10.1002/aic.690100217
Volland, J.-M., Gonzalez-Rizzo, S., Gros, O., Tyml, T., Ivanova, N., Schulz, F., Goudeau, D., Elisabeth, N.H., Nath, N., Udwary, D., Malmstrom, R.R., Guidi-Rontani, C., Bolte-Kluge, S., Davies, K.M., Jean, M.R., Mansot, J.-L., Mouncey, N.J., Angert, E.R., Woyke, T., Date, S.V.: A centimeter-long bacterium with DNA contained in metabolically active, membrane-bound organelles. Science **376**(6600), 1453–1458 (2022). https://doi.org/10.1126/science.abb3634
Watanabe, H., Iizuka, K.: The influence of dissolved gases on the density of water. Metrologia **21**(1), 19 (1985). https://doi.org/10.1088/0026-1394/21/1/005
Wen, Y.W., Kantzas, A.: Monitoring bitumen−solvent interactions with low-field nuclear magnetic resonance and x-ray computer-assisted tomography. Energy Fuels **19**(4), 1319–1326 (2005). https://doi.org/10.1021/ef049764g
Wigand, M., Kaszuba, J.P., Carey, J.W., Hollis, W.K.: Geochemical effects of CO_2 sequestration on fractured wellbore cement at the cement/caprock interface. Chem. Geol. **265**(1), 122–133 (2009). https://doi.org/10.1016/j.chemgeo.2009.04.008
Wise, D.L., Houghton, G.: The diffusion coefficients of ten slightly soluble gases in water at 10–60 °C. Chem. Eng. Sci. **21**(11), 999–1010 (1966). https://doi.org/10.1016/0009-2509(66)85096-0
Witherspoon, P.A., Saraf, D.N.: Diffusion of methane, ethane, propane, and n-butane in water from 25 to 43°. J. Phys. Chem. **69**(11), 3752–3755 (1965). https://doi.org/10.1021/j100895a017
Wollenweber, J., Alles, S., Kronimus, A., Busch, A., Stanjek, H., Krooss, B.M.: Caprock and overburden processes in geological CO_2 storage: an experimental study on sealing efficiency and mineral alterations. Energy Proc. **1**(1), 3469–76 (2009)
Zarghami, S., Boukadi, F., Al-Wahaibi, Y.: Diffusion of carbon dioxide in formation water as a result of CO_2 enhanced oil recovery and CO_2 sequestration. J. Pet. Exp. and Prod. Technol. **7**(1), 161–168 (2017). https://doi.org/10.1007/s13202-016-0261-7
Zivar, D., Kumar, S., Foroozesh, J.: Underground hydrogen storage: a comprehensive review. Int. J. Hydrogen Energy **46**(45), 23436–23462 (2021). https://doi.org/10.1016/j.ijhydene.2020.08.138

Authors and Affiliations

Saeed Khajooie[1,2] · Garri Gaus[1,4] · Timo Seemann[3] · Benedikt Ahrens[5] · Tian Hua[6] · Ralf Littke[1]

✉ Garri Gaus
garri.gaus@emr.rwth-aachen.de

[1] Institute of Organic Biogeochemistry in Geo-Systems, RWTH Aachen University, Lochnerstr. 4-20, Haus B, 52056 Aachen, Germany

[2] Institute of Applied Structural Geology, Teaching and Research Unit, RWTH Aachen University, Lochnerstrasse 4-20, 52056 Aachen, Germany

[3] Institute of Engineering Geology and Hydrogeology, RWTH Aachen University, Lochnerstrasse 4–20, 52056 Aachen, Germany

[4] Fraunhofer IEG – Fraunhofer Research Institution for Energy Infrastructures and Geothermal Systems, Kockerellstraße 17, 52062 Aachen, Germany

[5] Fraunhofer IEG - Fraunhofer Research Institution for Energy Infrastructures and Geothermal Systems, Am Hochschulcampus 1, 44801 Bochum, Germany

[6] Research Institute of Petroleum Exploration and Development, PetroChina, Beijing 100083, China